



UNIVERSITY OF LEEDS

This is a repository copy of *Carbon isotopes in clastic rocks and the Neoproterozoic carbon cycle*.

White Rose Research Online URL for this paper:
<http://eprints.whiterose.ac.uk/154595/>

Version: Accepted Version

Article:

Canfield, DE, Knoll, AH, Poulton, SW orcid.org/0000-0001-7621-189X et al. (2 more authors) (Cover date: February 2020) Carbon isotopes in clastic rocks and the Neoproterozoic carbon cycle. *American Journal of Science*, 320 (2). pp. 97-124. ISSN 0002-9599

<https://doi.org/10.2475/02.2020.01>

This is an author produced version of an article published in *American Journal of Science*.
Uploaded with permission from the publisher.

Reuse

Items deposited in White Rose Research Online are protected by copyright, with all rights reserved unless indicated otherwise. They may be downloaded and/or printed for private study, or other acts as permitted by national copyright laws. The publisher or other rights holders may allow further reproduction and re-use of the full text version. This is indicated by the licence information on the White Rose Research Online record for the item.

Takedown

If you consider content in White Rose Research Online to be in breach of UK law, please notify us by emailing eprints@whiterose.ac.uk including the URL of the record and the reason for the withdrawal request.



eprints@whiterose.ac.uk
<https://eprints.whiterose.ac.uk/>

Carbon isotopes in clastic rocks and the Neoproterozoic carbon cycle

Donald E. Canfield¹, Andrew H. Knoll², Simon W. Poulton³, Guy M. Narbonne⁴, Gregory R. Dunning⁵

¹Department of Biology and Nordcee, University of Southern Denmark, 5230 Odense M, Denmark

²Department of Organismic and Evolutionary Biology, Harvard University, Cambridge, MA 02138, USA.

³School of Earth and Environment, University of Leeds, Leeds LS2 9JT, UK

⁴Department of Geological Sciences and Geological Engineering, Queen's University, Kingston, ON, K7L 3N6, Canada

⁵Department of Earth Sciences, Memorial University of Newfoundland, St John's, Newfoundland, Canada A1B 3X5

Abstract

It has been proposed that isotopically light inorganic carbon precipitated diagenetically in clastic sediments can explain the large carbon isotopic excursions recorded in Neoproterozoic carbonates. To date, however, the data needed to test this hypothesis have been limited. Here we report the analysis of ca. 540 clastic sedimentary rocks, including shales, siltstones, sandstones and tillites that span the second half of the Neoproterozoic Era. A diagenetic carbon isotopic overprint does indeed occur in many of the samples; however, when we include our analyses in a carbon isotope mass balance model, they produce only a small effect on mass balance model results. Thus, clastic sedimentary rocks were not a major sink for ¹³C-depleted carbonate during the Neoproterozoic Era. These results do, however, produce a more accurate carbon mass balance, pointing to a high proportion of total organic carbon burial, compared to total carbon burial, during the late Tonian,

Cryogenian, and late Ediacaran Periods. This result suggests a vigorous release of oxygen to the atmosphere. The clastic carbonate record also offers a chemostratigraphic tool. For example, we observe an isotope trend in clastic-hosted carbonates of the Isaac Formation, Windermere Supergroup, that strongly resembles the Shuram-Wonoka isotope anomaly, allowing us to place this previously undated section in a temporal context. We also find isotope trends in the fossiliferous and radiometrically well-dated sedimentary rocks of the Avalon Peninsula, Newfoundland, that also may reflect the Shuram-Wonoka anomaly. If correct, this constrains the timing of the Shuram event, suggesting that it began after 571 Ma and ended before 562 Ma, with the most extreme isotopic values lying well within those bounds.

Introduction

In principle, the isotopic composition of carbon (both inorganic and organic) in sedimentary rocks provides recorded activities of the ancient carbon cycle (Bernier and Raiswell, 1983, Bjerrum and Canfield, 2011, Des Marais and others, 1992, Garrels and Lerman, 1981, Hayes, Strauss, and Kaufman, 1999). The basic premise is that inorganic carbon enters the oceans with an isotopic composition that is knowable ($\delta^{13}\text{C}_{\text{in}}$; a summary of term definitions is in Table 1). A fraction of this carbon is converted to organic carbon (f_{org}), with a distinct isotopic composition ($\delta^{13}\text{C}_{\text{org}}$) that is almost always ^{13}C -depleted compared to the isotopic composition of inorganic carbon ($\delta^{13}\text{C}_{\text{IC}}$) in the oceans. The burial of ^{13}C -depleted organic matter drives the $\delta^{13}\text{C}$ composition of the oceans ($\delta^{13}\text{C}_{\text{IC}}$) to more ^{13}C -enriched values compared to the input value ($\delta^{13}\text{C}_{\text{in}}$). An estimate of $\delta^{13}\text{C}_{\text{IC}}$ is obtained from sedimentary carbonates, while $\delta^{13}\text{C}_{\text{org}}$ is obtained from the isotopic composition of organic matter in sedimentary rocks. A simple mass balance equation can be written relating these parameters such that:

$$\delta^{13}\text{C}_{\text{in}} = \delta^{13}\text{C}_{\text{org}} f_{\text{org}} + \delta^{13}\text{C}_{\text{IC}} (1 - f_{\text{org}}) \quad 1)$$

Where the proportion of carbon buried as organic matter (f_{org}) can be calculated as:

$$f_{\text{org}} = (\delta^{13}\text{C}_{\text{IC}} - \delta^{13}\text{C}_{\text{in}}) / (\delta^{13}\text{C}_{\text{IC}} - \delta^{13}\text{C}_{\text{org}}) \quad 2)$$

If the input rate (flux_{in}) of inorganic carbon to the ocean is known or can be estimated (e.g. Bernier, 2004, Bernier and Raiswell, 1983, Garrels and Lerman, 1981), then burial fluxes of organic carbon in the past ($f_{\text{org}} * \text{flux}_{\text{in}}$) can be calculated. We note also that the burial of organic carbon into terrestrial sediments, of which coal formation is the most important sink (Bernier and Canfield, 1989), also impacts the isotopic mass balance of the carbon cycle (Bernier, 2004). However, our

analysis long predates the evolution of land plants and the deposition of coal, so we will ignore the terrestrial carbon cycle in what follows.

Along with pyrite sulfur, the burial flux of organic carbon into sediments is the ultimate source of oxygen to the atmosphere, so that the net input rate of oxygen into the atmosphere can be assessed from the carbon (and sulfur) isotope record (e.g. Berner, 2006, Canfield, 2005, Garrels and Perry, 1974). Furthermore, as the organic carbon buried in sediments ultimately comes from primary-producing organisms, the burial flux of organic carbon relates to the activity of the marine (and terrestrial, in so much as it contributes to organic carbon burial) biosphere through time (e.g. Berner, 2006, Bjerrum and Canfield, 2004a, Des Marais and others, 1992, Garrels and Perry, 1974, Hayes, Strauss, and Kaufman, 1999).

Thus, in principle, the isotopic record of carbon provides a valuable record of biosphere evolution and surface geochemistry through Earth history. Relative to the past 100 million years, the earlier record of sedimentary C isotopes is surprisingly variable, particularly for the Neoproterozoic Era, where carbonate $\delta^{13}\text{C}$ values are commonly more positive than those observed for recent times (e.g. Cox and others, 2016, Halverson and others, 2005, Hayes, Strauss, and Kaufman, 1999, Knoll and others, 1986, Macdonald and others, 2013) (Figure 1). Moreover, in Neoproterozoic sedimentary successions, the isotopic composition of inorganic carbon swings widely; on multiple occasions the $\delta^{13}\text{C}$ of marine carbonates reaches values less than the nominal input $\delta^{13}\text{C}_{\text{in}}$ value of -5‰ to -6‰ (Deines, 1980, Des Marais and others, 1992) (Figure 1). These large negative carbon isotope swings have received multiple explanations, including the transient oxidation of a large marine ^{13}C -depleted DOC pool (Rothman, Hayes, and Summons, 2003), the oxidation of a transient ^{13}C -depleted methane pulse, perhaps from the destabilization of a sediment methane-clathrate pool (Bjerrum and Canfield, 2011), and diagenetic alteration (Derry, 2010, Knauth and Kennedy, 2009, Swart and Kennedy, 2012).

While these large negative isotope shifts still lack a definitive explanation, late diagenetic alteration is perhaps the least likely alternative, at least for the Ediacaran Shuram-Wonoka anomaly (Figure 1), the largest negative carbon isotope swing in the geologic record. The Shuram-Wonoka anomaly has been identified globally (Grotzinger, Fike, and Fischer, 2011), and is remarkably consistent over large geographic areas (Grotzinger, Fike, and Fischer, 2011, Husson and others, 2015), requiring that processes responsible for the anomaly occurred globally at a unique point in time. The contemporaneous global coordination of a diagenetic event similar in style and magnitude seems unlikely. Furthermore, at least for the Shuram-Wonoka anomaly from the Adelaide Rift of South Australia, a late diagenetic source for the anomaly can be ruled out. Here, deep canyons formed adjacent to the depositing Wonoka Formation where the carbon isotope anomaly is found. Carbonate breccias in the canyons, derived from the Wonoka Formation, share the same color, lithofacies and isotopic compositions of in situ carbonates that form the canyon walls. These similarities strongly indicate that the carbon isotopic values of the breccias, and therefore of the carbonates of the Wonoka Formation, formed before the early reworking of Wonoka clasts (Husson, Maloof, and Schoene, 2012).

Following Equation 2, large positive carbon isotope excursions observed during the Neoproterozoic Era have traditionally been taken to reflect periods with a high proportion of organic matter burial (a large value for f_{org}) (Knoll and others, 1986). Several recent studies have come to challenge this idea by arguing that processes including photosynthesis and various types of diagenesis may act to decouple the carbon isotope record from the isotopic composition of seawater dissolved inorganic carbon ($\delta^{13}\text{C}_{\text{DIC}}$), thereby impacting the carbon isotope record ($\delta^{13}\text{C}_{\text{IC}}$) and its interpretation (Geyman and Maloof, 2019, Hoffman and Lamothe, 2019, Schrag and others, 2013). Thus, Hoffman and Lamothe (2019) have shown that Cryogenian-aged shelf deposits from the Otavi/Swakop platform preserve elevated $\delta^{13}\text{C}$ values compared to contemporaneous foreslope

deposits. In their interpretation, processes particular to the carbonate platform (see also Geyman and Maloof, 2019) elevated the $\delta^{13}\text{C}$ of the carbonates above seawater values. Furthermore, seawater-buffered diagenesis, driven by pore-water convection, altered the original $\delta^{13}\text{C}$ of the detrital carbonates in foreslope deposits to seawater values. In addition, isotopically light groundwaters provide an alternate source of diagenetic fluids (Wilson, 2005). Taken together, the isotopic composition of the platform deposits can be decoupled from the isotopic composition of seawater. The impact of these processes on the Neoproterozoic isotope record of $\delta^{13}\text{C}_{\text{IC}}$ will require further study, but we emphasize it is not critical that the carbonate isotope record represents the $\delta^{13}\text{C}$ of seawater DIC. Rather, it is critical that in estimating f_{org} , we identify the different sediment types contributing to isotope mass balance as developed more fully below.

In another recent study, Geyman and Maloof (2019) have shown that in modern shallow carbonates forming on Andros Island (Great Bahama Bank) and Shark Bay (western Australia) have $\delta^{13}\text{C}$ considerably in excess of seawater values. They argued that photosynthesis during the day draws down the local DIC pool, and with associated carbon-isotope fractionations, the $\delta^{13}\text{C}$ of carbonates precipitated during the day is ^{13}C -enriched compared to open seawater values. Furthermore, if nighttime organic matter respiration oxidizes photosynthetically-produced organic matter without accompanying carbonate precipitation, then ^{13}C -enriched carbonates form without accompanying organic matter burial. This can occur locally, but the extent to which this process would influence global isotope mass balance and interpretations of f_{org} depend on many factors. (It also raises the question why similar isotopic signatures are absent in carbonates deposited during the billion years prior to the Neoproterozoic record.) For example, this process would be of great significance if our reconstructions of the history of seawater $\delta^{13}\text{C}$ were based on a limited amount of carbonates formed in such a manner, but if most carbonates were formed elsewhere with a $\delta^{13}\text{C}$ resembling seawater, but somehow not included in the carbon isotope record (Geyman and Maloof,

2019). Conversely, if all carbonates formed in shallower environments with a $\delta^{13}\text{C}$ offset from seawater as described above, then the $\delta^{13}\text{C}$ carbonate record would be consistently ^{13}C -enriched compared to seawater. However, the precipitation of ^{13}C -enriched carbonates would leave seawater ^{13}C -depleted, and carbon mass balance would produce an identical f_{org} to the situation where no carbon isotope fractionation occurred during carbonate precipitation (Geyman and Maloof, 2019). Therefore, as discussed above in relationship to Hoffman and Lamothe (2019), it is not so important that the carbon isotope record reflects exactly the isotopic composition of seawater, but it is important that the isotope record reflects the isotopic composition of carbonate removed from seawater.

Therefore, we emphasize that in utilizing Equation 2 in constructing a carbon balance, one assumes that all carbon has been accounted for. In this regard, and with specific reference to the positive isotope excursions during the Neoproterozoic Era, (Schrag and others, 2013) have suggested that the large-scale early diagenetic formation of authigenic ^{13}C -depleted carbonates provides a previously unrecognized sink for ^{13}C -depleted carbonates—one not accounted for in Equation 2. The ^{13}C -depleted carbonate comes from organic matter oxidation, and if the sink is large enough, positive isotope excursions could be generated without reflecting large values of f_{org} . While ^{13}C -depleted authigenic carbonates are found today, they do not appear to be particularly important by mass (Schrag and others, 2013). However, Schrag and others (2013) argued that during Neoproterozoic times, with less oxygen in the atmosphere and oceans, aerobic organic matter mineralization in sediments would have been less important than today, resulting in a higher proportion of anaerobic mineralization. Anaerobic mineralization is more favorable for carbonate precipitation than aerobic mineralization (Canfield and Raiswell, 1991), possibly allowing for a greater extent of ^{13}C -depleted carbonate formation in Neoproterozoic-aged sediments. A large amount of ^{13}C -depleted diagenetic carbonate formation in sediments would potentially impact the

carbon isotope record and its subsequent interpretation. As explored in more detail below, however, such a mechanism of ^{13}C -enrichment would seemingly be controlled by factors other than widespread marine anoxia, as the ^{13}C -enrichment of marine carbonates was notably limited during the billion years preceding the Neoproterozoic Eon (e.g., Buick, Des Marais, and Knoll, 1995, Knoll, Kaufman, and Semikhatov, 1995), when marine anoxia was at least as widespread (Planavsky and others, 2011, Poulton and Canfield, 2011, Raiswell and Canfield, 2012, Scott and others, 2008, Wang and others, 2017). In what follows we will explore the proposal of (Schrage and others, 2013) making reference to other processes possibly influencing carbon isotope mass balance as described above (Geyman and Maloof, 2019, Hoffman and Lamothe, 2019).

Borrowing from Bjerrum and Canfield (2004b), Schrage and others (2013) introduced a second diagenetic component to the carbon mass balance such that:

$$\delta^{13}\text{C}_{\text{in}} = \delta^{13}\text{C}_{\text{org}} f_{\text{org-dc}} + (\delta^{13}\text{C}_{\text{IC}})(1 - f_{\text{org-dc}})(1 - f_{\text{dc}}) + \delta^{13}\text{C}_{\text{dc}}(1 - f_{\text{org-dc}})f_{\text{dc}} \quad 3)$$

where f_{dc} is the fraction of IC buried as diagenetic carbonate. From here, equation 3 can be solved for $f_{\text{org-dc}}$ (the f_{org} value obtained when considering diagenetic carbonates) yielding:

$$f_{\text{org-dc}} = \frac{\delta^{13}\text{C}_{\text{in}} - \delta^{13}\text{C}_{\text{IC}}(1 - f_{\text{dc}}) - f_{\text{dc}}\delta^{13}\text{C}_{\text{dc}}}{\delta^{13}\text{C}_{\text{org}} - \delta^{13}\text{C}_{\text{IC}} + f_{\text{dc}}(\delta^{13}\text{C}_{\text{IC}} + \delta^{13}\text{C}_{\text{dc}})} \quad 4)$$

As an example, Schrage and others (2013) calculated that a $\delta^{13}\text{C}_{\text{IC}}$ of 5‰ in the oceans could be maintained with $f_{\text{org-dc}} = 0.2$, the same as today, if f_{dc} lay between 0.29 and 0.37, with corresponding $\delta^{13}\text{C}_{\text{dc}}$ values of -15‰ and -10‰, respectively. In contrast, an f_{org} of 0.2 today generates a $\delta^{13}\text{C}_{\text{IC}}$ of 0‰ in the absence of significant diagenetic carbonate formation. Schrage and others (2013) further calculated that an f_{dc} of 0.33, representing 33% of the total modern carbonate burial flux of about

$7.5 \times 10^{14} \text{ g y}^{-1}$, would generate an average concentration of diagenetic IC of 1.5 wt% in clastic sedimentary rocks with a total terrestrial sediment flux of $1.7 \times 10^{16} \text{ g y}^{-1}$.

A record of diagenetic carbonate should be observable in the clastic sedimentary rock record. Note, however, that while diagenetic carbonates will be hosted in clastic sedimentary rocks, not all carbonate in clastic rocks need be diagenetic. Some of the carbonate could have originated by precipitation in, and settling from, overlying seawater, and some might be detrital. Furthermore, while seawater-derived carbonates should carry the seawater isotopic signal, there is no a priori isotopic value one can assign to diagenetic carbonates; they can exhibit values anywhere between seawater DIC and those approaching $\delta^{13}\text{C}_{\text{org}}$. In this way, it is difficult to isolate precisely the diagenetic component of clastic rock-hosted carbonates. Therefore, equation 5, as formulated, is difficult to use. However, if we recognize that diagenetic carbonates are part of the rock record of clastic sedimentary rocks, then we can recast equations 3 and 4 to provide a mass balance with clastic rock-hosted carbonates:

$$\delta^{13}\text{C}_{\text{in}} = \delta^{13}\text{C}_{\text{org}} f_{\text{org-cc}} + (\delta^{13}\text{C}_{\text{IC}})(1 - f_{\text{org-cc}})(1 - f_{\text{cc}}) + \delta^{13}\text{C}_{\text{cc}}(1 - f_{\text{org-cc}})f_{\text{cc}} \quad 5)$$

where $\delta^{13}\text{C}_{\text{cc}}$ is the isotopic composition of clastic-rock carbonate and f_{cc} is the fraction of IC buried as clastic rock-hosted carbonates. From here, equation 5 can be solved for $f_{\text{org-cc}}$ yielding:

$$f_{\text{org-cc}} = \frac{\delta^{13}\text{C}_{\text{in}} - \delta^{13}\text{C}_{\text{IC}}(1 - f_{\text{cc}}) - f_{\text{cc}}\delta^{13}\text{C}_{\text{cc}}}{\delta^{13}\text{C}_{\text{org}} - \delta^{13}\text{C}_{\text{IC}} + f_{\text{cc}}(\delta^{13}\text{C}_{\text{IC}} + \delta^{13}\text{C}_{\text{cc}})} \quad 6)$$

We emphasize that while clastic rock-hosted carbonates may represent a mix of both seawater-derived and diagenetic carbonates, they include the diagenetic component, and any isotopic deviations in the clastic rock record from expected seawater values (or values representing the carbonate isotope record) can be attributed to the diagenetic carbonate component in the rocks. However, not all diagenetic carbonates need deviate from seawater values, and the seawater isotope

mass balance as expressed in equations 5 and 6 will only be influenced by those that do. As isotopically distinct diagenetic carbonates should be part of the clastic rock isotope record, these will be revealed through analysis of clastic rock-hosted $\delta^{13}\text{C}$ carbonate values. In other words, we do not need to isolate the diagenetic component explicitly in order to evaluate its significance. We can demonstrate this through a simple mass balance calculation. For example, let us assume we have a true diagenetic carbonate contribution of 0.5 wt% IC with a $\delta^{13}\text{C}_{\text{cc}}$ of -10‰. With the IC burial and river fluxes presented in Schrag and others (2013) an f_{cc} of 0.11 is calculated (from equation 6), yielding an $f_{\text{org-cc}}$ of 0.14 together with the other standard parameters as presented in Table 2. A somewhat higher f_{org} of 0.173 is calculated (equation 2) without considering the burial of diagenetic carbonates. We assume now that the same amount of diagenetic carbonate is buried together with an equal amount of seawater-derived carbonate. In this case, the $\delta^{13}\text{C}_{\text{cc}}$ becomes -5‰ and the f_{cc} increases to 1 wt%, with no effect on the resulting $f_{\text{org-cc}}$ (Table 2). Thus, there is no need to isolate the pure diagenetic component of the carbonates buried with clastic rocks to determine the influence of diagenetic carbonates on the isotope mass balance.

With this in mind, we analyzed the isotopic compositions and concentrations of inorganic and organic carbon (in most cases) from 541 clastic rocks spanning the second half of the Neoproterozoic Era. Through these analyses we find clear evidence for a diagenetic $\delta^{13}\text{C}$ signal in many cases, but the concentrations of diagenetic carbonate are not high enough and their isotopic compositions not sufficiently ^{13}C -depleted to support the hypothesis that diagenetic carbonates have significantly influenced the isotopic expression of the marine carbon cycle. We also see that in some instances carbon isotope trends in clastic successions may be traceable to well-known isotope excursions, allowing possible stratigraphic correlation and dating in sequences with previously uncertain correlations and chronologies.

Materials and Methods.

The stratigraphic sequences reported here are the same as those previously reported in Canfield, Poulton, and Narbonne (2007) and Canfield and others (2008), drawing from splits of the same samples used in these previous studies. All organic carbon concentrations and isotopic compositions were determined on samples after decarbonation (0.5 M HCl overnight) using a Thermo Scientific Flash 2000 elemental analyzer coupled to a Thermo Fischer Delta Plus mass spectrometer. Concentrations of organic carbon were determined from the peak area recorded in the mass spectrometer, calibrated against a standard protein (46.5 wt% C) and a standardized internal sediment sample (6.72 wt% C). The uncertainty in the organic carbon concentrations varied depending on concentration, but is estimated as $\pm 15\%$ for the lowest concentrations reported here. Organic matter isotopic compositions are reported as $\delta^{13}\text{C}$ values relative to VPDB and were calibrated against NBS-19 ($\delta^{13}\text{C} = 1.95\text{‰}$), a lab urea standard standardized to $\delta^{13}\text{C} = -45.9\text{‰}$, and a lab sediment standardized to $\delta^{13}\text{C} = -26.07\text{‰}$. Maximum uncertainty is estimated at $\pm 0.5\text{‰}$.

The isotopic composition and concentrations of inorganic carbon were measured in two ways. In some cases, when there was sufficient inorganic carbon, the isotopic composition and concentrations of inorganic carbon were measured on untreated samples using an elemental analyzer, coupled to a mass spectrometer, as explained above. In this case, the isotopic compositions and concentrations of inorganic carbon were corrected for the typically small amount of organic carbon in the samples, as determined separately and as also outlined above. Uncertainty in concentrations are estimated as $\pm 5\%$, while uncertainty in isotope values are estimated as $\pm 0.5\text{‰}$. In most cases, however, the isotopic compositions and concentrations of inorganic carbon were determined on the CO_2 gas liberated into a closed container during the reaction of phosphoric acid for 24 hours at room temperature (Torres, Mix, and Rugh, 2005). In some cases, acid reaction was conducted on sample splits at 50°C for 24 hours with no significant difference in the results. The liberated CO_2 was introduced in triplicate with a Thermal Scientific Gas Bench II into a

Thermal Scientific Delta V plus mass spectrometer. Concentrations of inorganic carbon were calibrated from the peak area given by the mass spectrometer relative to the NBS-18 calcium carbonate standard with an uncertainty estimated as $\pm 5\%$. The isotopic compositions of inorganic carbon were calibrated relative to LSVEC ($\delta^{13}\text{C} = -46.48\text{‰}$) and NBS-18 ($\delta^{13}\text{C} = -5.01\text{‰}$) with a maximum uncertainty estimated as $\pm 0.5\text{‰}$. In many cases, the concentrations of inorganic carbon were very low, and values were not considered reliable unless triplicate analyses provided by the gas bench were consistent within a maximum difference of 1%. The isotopic composition of oxygen in the CO_2 ($\delta^{18}\text{O}$) is reported relative to VPDB and was standardized against LSVEC ($\delta^{18}\text{O} = -23\text{‰}$) and NBS-18 ($\delta^{18}\text{O} = -26.46\text{‰}$). The maximum uncertainty of these values is estimated as $\pm 1.0\text{‰}$, and values were not considered reliable unless the triplicate analyses were consistent to a maximum difference of 2%.

We also provide a new high-precision U-Pb date for the top of the Trepassy Formation of the Avalon Peninsula. The details of the dating procedure are described in the Appendix.

Results

The isotopic compositions and concentrations of inorganic and organic carbon are presented as time plots in Figure 2; formations sampled and their approximate ages are presented in Table 2. All data can be found in the Appendix, as can $\delta^{18}\text{O}$ values for the carbonates, included for completeness but not otherwise discussed. Also designated is the rock type of each sample. The database includes two types of sample sets. One set is derived from multiple formations that together span most of the later Neoproterozoic Era, but with low sampling density. The other includes selected formations sampled at much higher stratigraphic density. These include the Kaza and Isaac formations of the Cariboo Mountains, British Columbia, Canada; the Tapley Hill and Sturt Tillite formations of northern Australia; the Sheepbed and Twitya formations of the Mackenzie Mountains, Canada; and

a number of formations in stratigraphic succession from the Avalon Peninsula of Newfoundland. The formations with low data density help to establish the significance of diagenetic carbonates in Neoproterozoic-aged clastic rocks, while the formations with higher data density additionally reveal possible correlations between clastic rocks that host carbonates and stratigraphic patterns of carbon isotope change, as documented in Figure 1.

Discussion

As is obvious from Figure 1, $\delta^{13}\text{C}_{\text{IC}}$ trends during the Neoproterozoic Era are extremely dynamic, ranging over nearly 20‰ and with distinct behaviors that differ from one time interval to the next. As noted in the Introduction, there is an evolving and still open discussion as to how this isotope record reflects the history of the isotopic composition of seawater DIC. However, we also note that in many instances these isotopic trends are widely distributed (e.g. Cox and others, 2016, Halverson and others, 2005, Hayes, Strauss, and Kaufman, 1999, Knoll and others, 1986, Macdonald and others, 2013) and thus likely reflect a major portion of the carbonate precipitated from seawater. As these trends become refined and as a better understanding of the isotopic history of carbonate precipitation emerges, the results below can be modified to reflect this new understanding. For now, we assume that these isotopic trends reflect the isotopic history of the major inventory of carbonates precipitated from seawater. Our discussion will also proceed as if these trends represent the isotopic history of seawater DIC. As a matter of approach, to accommodate the isotope trends revealed in the “standard” isotope curve, we discuss distinct time bins individually, beginning with the later Tonian Period.

Tonian Period: Our data cover the later Tonian Period from about 835 to 725 Ma. During this time, the “standard” carbonate isotope record yields mostly positive $\delta^{13}\text{C}_{\text{IC}}$ values (Figure 1), but with decided swings to negative values during the so-called “Bitter Springs” anomaly around 800 Ma

and the subsequent Islay excursion now dated at about 735 Ma (MacLennan and others, 2018, Swanson-Hysell and others, 2015) (Figure 1; Halverson and others, 2005). We note that the Islay excursion is defined by nearly identical isotope trends from both Mackenzie Supergroup of western Canada and the Tambien Group of northern Ethiopia (MacLennan and others, 2018, Swanson-Hysell and others, 2015). Indeed, the Tonian carbon isotope record from 845 to the start of the Sturtian Glaciation at about 717 Ma is highly coherent when comparing data from Canada, Ethiopia, and Australia (Swanson-Hysell and others, 2015), suggesting that this record may well reflect the isotopic composition of carbonates precipitated from Tonian seawater.

Our clastic rock-hosted ($\delta^{13}\text{C}_{\text{cc}}$) data includes samples from the Bitter Springs Formation as well as the Quartzite, Multicolor and Limestone-Dolomite series, East Greenland. The ages of the latter successions are less well constrained, but the Quartzite and Multicolor successions antedate the Bitter Springs anomaly, suggesting an age range of 830-800 Ma. The Limestone Dolomite Series, in turn, contains the Bitter Springs anomaly near its base and the Islay excursion near its top (Knoll and others, 1986), suggesting an age of between 800 and 730 Ma.

Our clastic rock hosted $\delta^{13}\text{C}_{\text{cc}}$ values display similar ranges in $\delta^{13}\text{C}$ values to the standard isotope curve for the same interval (compare Figures 1 and 2), with prominently ^{13}C -enriched values, punctuated by the Bitter Springs and Islay excursions to moderately low values. That is, stratigraphic variations in the clastic rock-hosted record generally mirror those of carbonate successions, suggesting a strong influence of seawater IC on carbonates deposited within these clastic rocks. For the interval over which we have clastic rock $\delta^{13}\text{C}$ data (ca. 725 to 835 Ma), the average $\delta^{13}\text{C}_{\text{IC}}$ from the standard isotope record is 3.97‰ (Table 4). To obtain this average we first calculated mean $\delta^{13}\text{C}_{\text{IC}}$ values in 7-10 Ma bins (Figure 1), and then averaged these over the time interval of interest. The clastic rock-hosted record provides a weight-averaged $\delta^{13}\text{C}_{\text{cc}}$ value that is

nearly the same at 3.88‰, with an average IC concentration of 1.64 wt% (Table 3). The weight-averaged $\delta^{13}\text{C}_{\text{cc}}$ value is obtained from Equation 7 and is used because the influence of clastic-rock hosted $\delta^{13}\text{C}_{\text{cc}}$ values on isotope mass balance will depend on the concentration of IC in the clastic rock.

$$\delta^{13}\text{C}_{\text{ccave}} = \frac{\sum \delta^{13}\text{C}_{\text{cc}} * \text{wt}\% \text{ IC}}{\sum \text{wt}\% \text{ IC}} \quad 7)$$

If our late Tonian clastic rock data reflect clastic rocks in general from that time, then there is no indication that the burial of clastic rock-hosted diagenetic carbonates had significant influence on the seawater $\delta^{13}\text{C}_{\text{IC}}$ record. Thus, while the clastic rocks have an average concentration of 1.64% IC, similar to that predicted by Schrag and others (2013) for Neoproterozoic Era diagenetic carbonates, the isotopic composition of clastic rock-hosted IC is nearly identical to seawater values and thus cannot account for the ^{13}C -enriched seawater values observed at this time. One might argue that the carbonates in our clastic samples are in fact depositional and not diagenetic, but to the extent that this is true, it simply decreases the abundance of diagenetic carbonate, again supporting the view that this pool is not strongly affecting seawater composition.

If we accept that the majority of carbonates in our clastic rocks were derived either from water column or diagenetic precipitation, we can determine how the clastic rock carbonate record influences our interpretation of the carbon isotope record. We do this by utilizing equation 6. With a clastic rock average carbonate content of 1.64 wt% IC, an f_{cc} of 0.37 is calculated using the total carbonate burial rates and sedimentation from rates from Schrag and others (2013). This value of f_{cc} implies that 37% of the carbonate in late Tonian times was buried in association with clastic rocks. Thus, utilizing our calculated value of f_{cc} along with an average $\delta^{13}\text{C}_{\text{oc}}$ from our isotope record (-30.04‰: Figure 2, Table 4) we obtain an $f_{\text{org-cc}}$ from equation 6 of 0.262 (Table 4), nearly the same to the f_{org} of 0.264 calculated without considering diagenetic carbonate burial. Therefore, our data

suggest that for the late Tonian Period, ^{13}C -enrichments in seawater carbonates reflect a high proportion of organic carbon burial (high f_{org}) without an obviously strong influence from diagenetic carbonates.

Cryogenian Period

The interglacial Cryogenian rock record is estimated to have extended from about 660 to 645 Ma (Hoffman and others, 2017). Our clastic rock record from this time includes sediments from the Tapley Hill Formation from northern Australia, as well as shales and sands within the upper part of the underlying Sturt Tillite, the Twitya Formation from western Canada, the Tillite Group from East Greenland, and the Elbobreen Formation from Spitsbergen (Table 3), all estimated to range in age from 652 to 650 Ma, the earlier half of the Cryogenian Period. In this time interval, both platform and foreslope deposits as analyzed by (Hoffman and Lamothe, 2019) share nearly identical carbon isotopic compositions, and compositions similar to the standard curve (Figure 1), suggesting that in this time window the standard curve reflects the carbon isotopic composition of seawater DIC.

In contrast to our late Tonian samples, there is a strong a diagenetic influence in some of these sedimentary rocks. For example, $\delta^{13}\text{C}_{\text{cc}}$ values for the Twitya Formation vary between 3‰ to -10‰ (Table A1), with most values distinctly ^{13}C -depleted relative to lower Twitya carbonates (-1 to -3‰) (Kaufman, Knoll, and Narbonne, 1997) and to the standard isotope curve (compare Figures 1 and 2). The disparity between the clastic sediment-hosted and standard isotope curve, however, becomes most apparent when we calculate isotope averages. Thus, a weighted average $\delta^{13}\text{C}_{\text{cc}}$ of 0.94‰ (from equation 7) is compared to a seawater average $\delta^{13}\text{C}_{\text{IC}}$ of 4.17‰ calculated for the first half of the Cryogenian interglacial interval; a time interval corresponding to our samples (Figures 1, 2 and Table 4). The average concentration of clastic rock-hosted carbonate is 2.02 wt%, which translates to an f_{cc} of 0.45 with the carbonate fluxes and sedimentation rates as given above and in

(Schrag and others, 2013). We also calculate an average $\delta^{13}\text{C}_{\text{oc}}$ of -29.14‰ from the Cryogenian clastic rocks (Figure 2 and Table 4), and from these values, we calculate using equation 6 an $f_{\text{org-cc}}$ of 0.242 that includes the influence of diagenetic carbonate burial. From equation 2, an f_{org} of 0.275 is calculated from the same input values but without the influence of diagenetic carbonates. Thus, in the interglacial Cryogenian Period, the burial of diagenetic carbonates appears to have had a small (0.242 vs. 0.275) influence calculated values of f_{org} .

We also consider how the burial of diagenetic carbonates has influenced the $\delta^{13}\text{C}_{\text{IC}}$ of seawater. Thus, as calculated above, the complete isotope mass balance, including the influence of diagenetic carbonates, is consistent with an $f_{\text{org-cc}}$ of 0.242. This $f_{\text{org-cc}}$ value is calculated together with the actual average seawater $\delta^{13}\text{C}_{\text{IC}}$ of 4.17‰. The same value of f_{org} , but without diagenetic carbonate burial, is consistent with a $\delta^{13}\text{C}_{\text{IC}}$ of 2.72‰ (Table 4). This value is calculated by rearranging equation 1 to:

$$\delta^{13}\text{C}_{\text{IC}} = (\delta^{13}\text{C}_{\text{in}} - \delta^{13}\text{C}_{\text{org}} f_{\text{org}})/(1 - f_{\text{org}}). \quad 8)$$

Therefore, the burial of diagenetic carbonates in the first half of the interglacial Cryogenian Period raised the $\delta^{13}\text{C}_{\text{IC}}$ of seawater by about 1.5‰ (from 2.72‰ to 4.17‰). While significant, this effect is still relatively modest and much smaller than the > 5‰ effects suggested by (Schrag and others, 2013).

Ediacaran Period

The Ediacaran Period reflects a time of widely varying seawater $\delta^{13}\text{C}_{\text{IC}}$ values (Figure 1), including the prominent Shuram-Wonoka excursion, estimated here to have occurred some 570-560 Ma (as discussed more fully below). Once again, successions distributed around the world, including

northwestern Canada, south China, Oman, Namibia, and Australia, yield closely similar C-isotopic stratigraphies (Macdonald and others, 2013).

Due to the high variability in the Ediacaran Period isotope record, we have elected to analyze this record in three intervals: pre-Shuram-Wonoka anomaly (636-570 Ma), the postulated 10 million years encompassing the Shuram-Wonoka anomaly (570-560 Ma; see below) and post Shuram-Wonoka (560-541 Ma). We believe that the age assignments for the sections used to generate our clastic-hosted $\delta^{13}\text{C}_{\text{cc}}$ are robust enough to justify these coarse time bins; see Table 3). However, we also analyzed all Ediacaran data together.

Beginning with pre-Shuram-Wonoka time interval (636-570 Ma), it is clear that diagenetic carbonates are a part of the clastic-hosted carbonate record when comparing $\delta^{13}\text{C}_{\text{IC}}$ (1.32‰) to $\delta^{13}\text{C}_{\text{cc}}$ (-2.82‰) (Table 4). However, the concentrations of carbonate are relatively low (0.42 wt%), and overall, by including clastic carbonates, f_{org} only changes a relatively small amount from a value of 0.201 to an $f_{\text{org-cc}}$ of 0.189 when considering the influence of the clastic carbonate on the isotope mass balance (Table 4). During the Shuram-Wonoka interval (570 to 560 Ma) many of the clastic-hosted carbonates have very low $\delta^{13}\text{C}_{\text{cc}}$ values of down to -27‰ (Figures 2 and 5, if our age assignments for the Avalon Peninsula are correct, as discussed below). But still, despite these low values reflecting a clear diagenetic effect, the average $\delta^{13}\text{C}_{\text{cc}}$ of -1.81‰ for the period between 570 and 560 Ma is surprisingly greater than the average $\delta^{13}\text{C}_{\text{IC}}$ (-6.55‰) (Table 4). The reason for this is that the low $\delta^{13}\text{C}_{\text{cc}}$ values are accompanied by very low carbonate concentrations that do little to influence the average $\delta^{13}\text{C}_{\text{cc}}$ of the interval, which is heavily influenced by rocks deposited outside of the nadir of the anomaly, and with higher carbonate content and elevated $\delta^{13}\text{C}_{\text{cc}}$ values. Therefore, on average for the time interval between 570 to 560 Ma, diagenetic carbonates have no significant influence on the calculation of f_{org} (Table 4). For rocks deposited after the Shuram-

Wonoka anomaly, diagenetic carbonates are quite prominent with an average $\delta^{13}\text{C}_{\text{cc}}$ of -7.97‰ compared to an average $\delta^{13}\text{C}_{\text{IC}}$ of 2.91‰ . But again, despite low average $\delta^{13}\text{C}_{\text{cc}}$ for diagenetic carbonates during this time interval, their influence on isotope mass balance is almost negligible due to a low clastic rock carbonate content of only 0.12 wt% (Table 4). Taken together, the influence of diagenetic carbonates on the carbon isotope mass balance during the Ediacaran Period is also quite small (Table 4).

Neoproterozoic Era

Having examined isotopic data for discrete intervals of Neoproterozoic time, we can step back and evaluate the influence of diagenetic carbonates across the entire interval under consideration. Our analysis is the same as above for individual Neoproterozoic time intervals (see calculation values in Table 4). Taking all the Neoproterozoic data together, a $\delta^{13}\text{C}_{\text{IC}}$ of 2.82‰ is calculated from the standard isotope curve (from 835-541 Ma, the same age range as represented in our clastic rock-carbonate data; Figure 1), and a concentration-weighted average $\delta^{13}\text{C}_{\text{cc}}$ of 0.93‰ as calculated from data in Figure 2. We also calculate an average clastic rock carbonate content of 1.13 wt%, and this translates into an f_{cc} of 0.252 with the same values of total carbonate burial and sedimentation rates as described above and as given in (Schrag and others, 2013). With an average $\delta^{13}\text{C}_{\text{OC}}$ of -30.16‰ from data in Figure 2, an $f_{\text{org-cc}}$ of 0.226 is calculated and compared to an f_{org} of 0.237 in the absence of diagenetic carbonates. Likewise, with an $f_{\text{org-cc}}$ of 0.237, a $\delta^{13}\text{C}_{\text{IC}}$ of 2.34‰ is calculated from equation 2 and demonstrates that over all of the Neoproterozoic Era, diagenetic carbonates have had the effect of increasing $\delta^{13}\text{C}_{\text{IC}}$ from 2.34‰ to 2.82‰ – a relatively small amount.

As noted above, it can be difficult to isolate the influence of diagenetic carbonates on the clastic rock carbonate pool, as this pool likely does not have a distinct isotope signature.

Nevertheless, we attempt to see whether an obvious diagenetic carbon isotope signal is related to

parameters that might be a proxy for the extent of anaerobic diagenesis as this has been proposed to encourage diagenetic carbonate precipitation (Schrag and others, 2013). First, we explore the relationship between $\delta^{13}\text{C}_{\text{cc}}$ and TOC, as higher concentrations of TOC might be expected to drive more extensive anaerobic diagenesis. Our data show (Figure 3A) that the most ^{13}C -depleted carbonates are found at low concentrations of TOC. Indeed, the samples with the clearest diagenetic origin (with $\delta^{13}\text{C}_{\text{cc}} < -12\text{‰}$) are mostly found at concentrations of TOC < 0.1 wt%. While these trends cannot rule out a diagenetic influence in clastic rock-hosted carbonate production, they are counter to the expectation that higher degrees of anaerobic diagenesis, driven by high concentrations of TOC, lead to more abundant ^{13}C -depleted diagenetic carbonates.

We also compared our $\delta^{13}\text{C}_{\text{cc}}$ data to earlier determinations of highly reactive to total iron (FeHR/FeT) for these same rocks (Canfield and others, 2008, Canfield, Poulton, and Narbonne, 2007). When FeHR/FeT exceeds 0.38, there is indication of deposition under anoxic water column conditions (Raiswell and Canfield, 1998, Raiswell and Canfield, 2012), and this should enhance the prospects for anaerobic sediment diagenesis. We find (Figure 3B) little evidence for enhanced deposition of ^{13}C -depleted carbonates at high values of FeHR/FeT. Indeed, the lowest values of $\delta^{13}\text{C}_{\text{cc}}$ are found when FeHR/FeT is < 0.38 , providing no indication of an anoxic water column. We also see this when looking at the specific isotope trends in the Cariboo Mountains, western Canada (Figure 4). Here, we see that the most ^{13}C -depleted carbonate values are found in the deep-water sedimentary rocks of the Kaza Formation (Cochrane, Navarro, and Arnott, 2019) which also display low ratios of FeHR/FeT (see also, Raiswell and Canfield, 2012). In contrast, deltaic sedimentary rocks of the Isaac Formation display many values of FeHR/FeT elevated above 0.38, consistent with anoxic depositional conditions, but with less ^{13}C -depleted carbonates. These isotope trends, and particularly those from the Isaac Formation, are discussed in more detail below.

The one exception is data from the Cryogenian Period, where the lowest $\delta^{13}\text{C}_{\text{cc}}$ values are found at high FeHR/FeT values. These data come from the Twitya Formation, and here, as discussed above, ^{13}C -depleted diagenetic carbonates clearly formed. However, the Twitya Formation seems to be the exception rather than the rule, and overall, there is little indication that anoxic water column conditions increased the prospect of forming ^{13}C -depleted diagenetic carbonates during the Neoproterozoic Era.

Carbon burial and oxygen production

We conclude that averaged over all of the Neoproterozoic Era, diagenetic carbonates had a relatively small influence on the seawater isotope mass balance. Still, the most accurate mass balance includes the influence of diagenetic carbonates as reflected in our clastic rock analyses. With these analyses, the resulting calculated values (Table 4) show that $f_{\text{org-cc}}$ was elevated relative to today for much of later Neoproterozoic time. It is also clear that much of the Neoproterozoic carbon isotope record has been influenced by non-steady-state processes, with excursions to highly ^{13}C -depleted values that are still poorly understood (e.g., (Bjerrum and Canfield, 2011, Rothman, Hayes, and Summons, 2003), so its interpretation requires care. Nonetheless, even if large negative ^{13}C excursions may be promoted by non-steady-state marine DOC oxidation (Rothman, Hayes, and Summons, 2003) or periods of rapid methane release (Bjerrum and Canfield, 2011), over long time intervals exceeding the residence of carbon in the atmosphere and oceans, isotope mass balance should hold as long as the source terms to the ocean remain the same and the sinks can be evaluated. This being the case, and if we have identified the most important long-term carbon sinks (marine DOC and methane clathrate hydrate accumulation represent transient reservoirs and not long-term sinks), the $f_{\text{org-cc}}$ values we have calculated may be representative of the long time intervals over which they have been averaged. If this is true, then, in line with earlier discussions,

the later Tonian to pre-Ediacaran isotope record is consistent with elevated rates of carbon burial and net oxygen release to the atmosphere compared to today (Knoll and others, 1986).

The Ediacaran Period is more difficult to evaluate. Averaged through the whole of the period, carbon mass balance suggests that organic carbon was buried in a proportion to total carbon burial ($f_{\text{org-cc}} = 0.185$) similar to today ($f_{\text{org}} = 0.2$). Ignoring the influence of pyrite burial on net oxygen release, a process that is still poorly studied (e.g. Canfield, 2005), oxygen release to the atmosphere during the Ediacaran Period would appear to have been similar to today. Our data also suggest that organic carbon burial during the latter part of the Ediacaran Period was more vigorous ($f_{\text{org-cc}} = 0.231$ from 541 to 560 Ma) than the time preceding, seemingly corresponding with evidence for increasing ocean oxygenation after the Gaskiers glaciation (Canfield, Poulton, and Narbonne, 2007, Von Strandmann and others, 2015), and the post-Gaskiers emergence of large Ediacaran animals (Bobrovskiy and others, 2018, Narbonne, 2005) that may have required elevated oxygen levels for their metabolism (Knoll, 2014). Our conclusion of relatively vigorous late-Ediacaran production of oxygen contrasts with earlier calculations revealing relatively low rates of oxygen production (e.g., Bjerrum and Canfield, 2004a, Canfield, 2014). These earlier calculation results were a product of previous age models suggesting that the Wonoka-Shuram anomaly was much longer in duration than we advocate here. We also note that the influence of oxygen release to the atmosphere during the late Tonian and Cryogenian Periods on ocean chemistry and the state of biological evolution remains a topic of active debate (e.g., Mills, Francis, and Canfield, 2018, Planavsky and others, 2014, Sperling, Knoll, and Girguis, 2015, Sperling and Stockey, 2018).

Individual carbon isotope records

While diagenesis has clearly influenced the $\delta^{13}\text{C}_{\text{cc}}$ of many Neoproterozoic samples analyzed here, comparison between Figure 1 and Figure 2A suggests that the $\delta^{13}\text{C}_{\text{cc}}$ record may follow the

standard curve in many cases. Thus, both records show strongly negative $\delta^{13}\text{C}$ values associated with the Bitter Springs and Islay anomalies, and even more pronounced negative values cluster in the mid-Ediacaran Period. Thus, while diagenesis has clearly influenced the $\delta^{13}\text{C}_{\text{cc}}$ of many Neoproterozoic samples analyzed here, clastic-rock carbonates may still provide insight into stratigraphic correlations among sites with limited or uncertain age constraints. Two examples are outlined below.

Cariboo Mountains

The Kaza and Isaac Formations of the Windermere Supergroup, British Columbia, Canada, represent a depositional environment that transited upward from deep-water basinal turbidites of the Kaza Formation to slope facies of the Isaac Formation. The Isaac Formation contains a mixture of turbiditic mudstones, siltstones, sandstones and conglomerates, with deeply incised channel deposits demonstrating active downslope sediment transport (Arnott and Ross, 2007, Cochrane, Navarro, and Arnott, 2019, Navarro, Khan, and Arnott, 2007, Ross, Bloch, and Krouse, 1995). The lowermost Isaac Formation contains the “First Isaac Carbonate” (FIC), a carbonate-rich unit of approximately 200 m thickness where the carbonates were sourced from a combination of carbonate clastics derived from an upslope carbonate platform and authigenic carbonate precipitates (Cochrane, Navarro, and Arnott, 2019). Overall, the depositional system of the Isaac Formation is enormous and has been compared in size to the current Amazon Delta (Arnott and Ross, 2007). Previous iron-speciation analyses are consistent with the Kaza Formation having deposited under oxygenated bottom water conditions, with the Isaac Formation having deposited under anoxic, mostly ferruginous, oxygen-minimum zone-like conditions (Canfield and others, 2008, Raiswell and Canfield, 2012). These formations are of Ediacaran age (Kendall and others, 2004), but more refined age constraints do not exist.

Recently, Cochrane, Navarro, and Arnott (2019) conducted a detailed analysis of the carbonate sources and diagenetic history of carbonates in the FIC unit. The FIC is a carbonate-rich unit containing a mixture of both detrital and authigenic carbonate phases, where the detrital carbonates were recrystallized from an upslope carbonate platform source. These were the most abundant carbonate phases and where the focus of the study. Their isotopic compositions showed smooth trends with $\delta^{13}\text{C}$ values reaching up to 3‰ to 4‰, leading (Cochrane, Navarro, and Arnott, 2019) to conclude that these likely represented seawater values and not a late diagenetic source where more ^{13}C -depleted values might be expected. Their results also demonstrate relatively ^{13}C -depleted values of around -5‰ in both the upper and lower parts of the FIC unit. These data, combined with elevated values in the middle of the interval, led Cochrane, Navarro, and Arnott (2019) to tentatively correlate the negative isotope excursions in the base of the FIC to the EN2 isotope excursion described from south China (McFadden and others, 2008). The EN2 itself has been tentatively associated with the Gaskiers Glaciation (Macdonald and others, 2013, Narbonne, Xiao, and Shields, 2012). Our results from the FIC agree well with those reported by Cochrane, Navarro, and Arnott (2019) (Figure 4). We also note that clastic-hosted carbonates from the Kaza Formation are highly ^{13}C -depleted, with values as low as -20‰; these likely reflect a diagenetic overprint. In contrast, for sediments deposited from the top of the FIC and further up-section, isotope trends, both in magnitude and form, are nearly indistinguishable from those observed for the Shuram anomaly from Oman (Fike and others, 2006). These isotope trends persist despite depositional lithologies ranging from silty turbidites to massive conglomeritic to sandy channel deposits (Figure 4). We are uncertain whether the carbonates in this interval of the Isaac formation are detrital or diagenetic and origin. We are certain, however, that the isotope trends transcend lithology, and we conclude that the Isaac formation records the Shuram-Wonoka isotope anomaly, providing a relative datum for these sediments and further demonstrating that this isotope anomaly

was global in scope (Husson and others, 2015). Our analysis demonstrates, furthermore, that $\delta^{13}\text{C}_{\text{cc}}$ isotopic trends may be useful in establishing stratigraphic correlations in ancient clastic rocks that are otherwise poorly dated.

Neoproterozoic of the Avalon Peninsula

The Conception and St. John's groups in the Avalon Peninsula of southeastern Newfoundland comprise a 6 km-thick succession of deep-water strata that pass upwards from basin plain to slope to delta-front environments (Canfield, Poulton, and Narbonne, 2007, Gardiner and Hiscott, 2003, Gehling, Narbonne, and Anderson, 2000, Wood, 2003). With the exception of the glacial diamictites of the Gaskiers Formation (Eyles and Eyles, 1989) near the base of the succession, these strata comprise a monotonous succession of mainly fine-grained, distal turbidites and shales that show no evidence of either emergence or storm waves. These strata are remarkable in containing the earliest known Ediacara-type fossils, including the well-known diverse fossil assemblages of Mistaken Point (Liu, Kenchington, and Mitchell, 2015, Narbonne, 2005). These rocks are also well dated, including a precise date of 579.44 ± 0.44 Ma for the end of Gaskiers Glaciation, and a variety of other dates, including 570.94 ± 0.38 Ma for an ash in the uppermost Drook Formation, 566.25 ± 0.35 Ma for the fossiliferous E-surface of the Mistaken Point Formation (Pu and others, 2016), and a new date of 562.5 ± 1.1 Ma near the top of the Trepassey Formation (see Appendix). This time frame would seem to be well suited for evaluating the chronology of the Shuram-Wonoka $\delta^{13}\text{C}$ isotope excursion. Indeed, previous dating in China reveals that the nadir of the Shuram-Wonoka must be older than 551.1 ± 0.7 Ma, where the nadir is separated from this dated horizon by an unconformity (Condon and others, 2005). There is some evidence from isotope trends that the anomaly ends stratigraphically below the unconformity (Condon and others, 2005), suggesting that the event was finished by 551 Ma at the youngest. However, a recent U-Pb date of 557 ± 3 Ma for a bentonite in the overlying Denying Formation suggests an older age for the end of the Shuram

excursion (Zhou and others, 2018). Furthermore, from broad global stratigraphic correlations, (Macdonald and others, 2013) concluded that the Shuram-Wonoka anomaly began well after the Gaskiers glaciation; they suggest a date of 565 ± 3 Ma for its beginning.

Our $\delta^{13}\text{C}_{\text{cc}}$ results for the Avalon Peninsula are presented in Figure 5, along with existing radiometric dates and relative formation thicknesses based on measured stratigraphic thickness as presented in O'Brien and King (2005). Generally, $\delta^{13}\text{C}_{\text{cc}}$ values are highly ^{13}C -depleted and show evidence for a diagenetic IC source. However, on top of this diagenetic influence, there are two prominent negative isotope excursions. One is found in the upper Mall Bay Formation, just prior to the Gaskiers glaciation, and the other extends from the middle of the Briscal Formation through the Trepassey Formation. The earlier excursion is generally consistent with suggestions for the timing of the EN2 isotope excursion (e.g., Macdonald and others, 2013, Narbonne, Xiao, and Shields, 2012, Xiao and others, 2016) as found in south China (McFadden and others, 2008). If true, then the EN2 excursion was likely a global phenomenon and clearly predated the Gaskiers glaciation. We suggest that the younger of these excursions represents the Shuram-Wonoka anomaly where diagenetic carbonates were formed from diagenetically impacted seawater already highly depleted in ^{13}C . Indeed, there is nothing in the post-Trepassey $\delta^{13}\text{C}_{\text{cc}}$ record to suggest the influence of a highly ^{13}C -depleted seawater source on clastic carbonate formation, as might be expected if the Shuram-Wonoka anomaly was younger than 562.5 Ma as constrained in Figure 5 and older than the recent 557 Ma date for post-Shuram-Wonoka beds in China (Zhou and others, 2018). If correct, the Shuram-Wonoka likely ended by post-Trepassey times.

There are highly ^{13}C -depleted clastic carbonates in the Drook and Trepassey formation, but nothing depleted to the same extent as those found in the upper Birscall and Mistaken Point formations. Therefore, based on our radiometric constraints, we suggest that the Shuram-Wonoka isotope anomaly began after 571 Ma and was over by 562.5 Ma, with the most extreme excursion

occurring well within this bounding range. The U-Pb zircon date within the Mistaken Point Formation (Fig. 5) additionally constrain the end of the excursion to lie between 566.25 \pm 0.35 Ma and 562.5 \pm 1.1 Ma. Our suggestion of a start after 571 Ma is generally consistent with the correlations made by Macdonald and others (2013), and a duration of 4-6 million years would be consistent with estimates for the duration of the isotopic event based on magnetic stratigraphy and cyclostratigraphy (Minguez, Kodama, and Hillhouse, 2015).

Our results also suggest that the Shuram-Wonoka-EN3 isotope excursion coincided with the acme of the Avalon assemblage of the Ediacara biota, as typified by the diverse rangeomorph fossils of the Mistaken Point Formation (Liu, Kenchington, and Mitchell, 2015, Narbonne, 2005). Less diverse examples of the Avalon assemblage pre-date the Shuram anomaly in the underlying Drook Formation in Avalonian Newfoundland and in the Nadaleen Formation (“June beds”) in NW Canada (Macdonald and others, 2013, Narbonne and others, 2014). Abundant bilaterian burrows and body fossils of the White Sea and Nama assemblages postdate the end of the Shuram anomaly worldwide.

Conclusions

We have analyzed the $\delta^{13}\text{C}$ of carbonates from 541 clastic rock samples spanning nearly the whole of the later Neoproterozoic Era. Most of these carbonates are found in very low concentration and many of them likely originated during early diagenesis. Indeed, many of the clastic rock-hosted carbonates have highly ^{13}C -depleted isotope values indicating a diagenetic origin. We constructed a carbon isotope mass balance to determine whether these clastic rock-hosted carbonates, not normally included in carbon isotope mass balance calculations, influence our understanding of the evolution of the carbon cycle. We conclude, first, that including clastic rock-hosted carbonates in mass balance calculations is the most correct approach to constructing a carbon isotope mass

balance. But, we also conclude that including the clastic rock-hosted carbonates only minimally alters the mass-balance results obtained in their absence. Thus, whilst being the most correct approach, including clastic rock-hosted carbonates does not substantially alter our understanding of the Neoproterozoic carbon cycle, nor do they explain the large isotope excursions found in Neoproterozoic carbonate rocks. Our mass balance results, however, do reinforce the idea that during Tonian and Cryogenian and Late Ediacaran times organic carbon was buried in a higher proportion to total carbon than at present, potentially generating a more vigorous source of atmospheric oxygen than today and possibly explaining the emergence of large Ediacaran Fauna after the Gaskiers Glaciation. We also emphasize that clastic-hosted carbonates seem to provide an untapped data repository that may facilitate allowing possible stratigraphic correlation of previously undated clastic sedimentary sequences.

Acknowledgements

We acknowledge the expert advice of Laura Bristow and the technical skills of Lilian Salling, Susanne Møller and Dina Skov Petersen. We are grateful to two anonymous reviewers and C. Page Chamberlain for valuable comments. We also acknowledge financial support from the Villum Foundation (grant 16518). AHK thanks the NASA Astrobiology Institute. SWP acknowledges financial support from a Royal Society Wolfson Research Merit Award and a Leverhulme Research Fellowship. GMN acknowledges funding from Natural Sciences and Engineering Research Council of Canada (NSERC) Discovery Grant 05561-2014, a Queen's University Research Chair, and field assistance from Kelsey Grimes and Nicole Heikoop. We are grateful to Galen Halverson, Dylan Cochrane, Nicholas Swanson-Hysell, Scott MacLennan and Francis Macdonald for sharing their carbon isotope databases. Work at the Mistaken Point Ecological Reserve was carried out under

Scientific Research Permits granted by the Parks and National Areas Division, Government of Newfoundland and Labrador. We thank Dr. Richard Thomas for his assistance and oversight.

Table 1. Definition of terms

Parameter	Definition
$\delta^{13}\text{C}_{\text{in}}$	Isotopic composition of inorganic carbon entering oceans
$\delta^{13}\text{C}_{\text{IC}}$	Isotopic composition of inorganic carbon in the oceans from “standard” isotope curve
$\delta^{13}\text{C}_{\text{org}}$	Isotopic composition of organic carbon in sedimentary rocks
$\delta^{13}\text{C}_{\text{dc}}$	Isotopic composition of diagenetic carbonates
$\delta^{13}\text{C}_{\text{cc}}$	Isotopic composition of clastic-rock carbonate
f_{org}	Fraction of total carbon buried as organic carbon
$f_{\text{org-dc}}$	Value of f_{org} when considering diagenetic carbonates
f_{cc}	Fraction of inorganic carbon buried as clastic carbonates
f_{dc}	Fraction of carbonate buried as diagenetic carbonates
$f_{\text{org-cc}}$	Value of f_{org} when considering clastic carbonates
flux_{in}	Flux of inorganic carbon to the oceans

Table 2. Influence of mixing “diagenetic” and seawater carbonate on f_{org} .

Parameter	100% diagenetic carbonate: 0% seawater carbonate	50% diagenetic carbonate: 50% seawater carbonate
$\delta^{13}\text{C}_{\text{cc}}$	-10 ‰	-5 ‰
$\delta^{13}\text{C}_{\text{OC}}$	-28.9 ‰	-28.9 ‰
$\delta^{13}\text{C}_{\text{IC}}$	0 ‰	0 ‰
wt% IC	0.5	1.0
f_{cc}	0.11	0.22
$f_{\text{org-cc}}$	0.140	0.140
f_{org}	0.173	0.173

Table 3. Formations, locations and approximate ages for samples from this study

Formation	Location	Depositional Setting	Estimated Age (Ma)
Bitter Springs	Amadeus Basin, Australia	SS	800-812
Quartzite Series	East Greenland	SS	820-830
Multicolor Series	East Greenland	SS	810-820
Limestone-Dolomite Series	East Greenland	SS	730-770
Tapley Hill	South Australia	OS	652-658
Apilla/Sturt Tillite	South Australia	OS	658-660
Elbobreen	Spitzbergen	OS	652-660
Dracoisen	Spitzbergen	OS	610-620
Tillite Group	East Greenland	OS	632-635
Canyon Formation	East Greenland	SS	620-630
Spiral Creek	East Greenland	SS	600-620
Woomera	Stuart Shelf, South Australia	SS	625
Arcoona ABC	Stuart Shelf, South Australia	SS	620
Elyuah	Stuart Shelf, South Australia	OS	610
Grants Bluff	Stuart Shelf, South Australia	OS	590
Upper Kaza	Caribou Mtns, western Canada	DB	569.9-571.8
Isaac	Caribou Mtns, western Canada	DB	562.3-569.8
Twitya	Mackenzie Mtns, western Canada	DB	652-660
Sheepbed	Mackenzie Mtns, western Canada	DB	596-625
Mall Bay	Avalon Peninsula, Newfoundland	DB	581.9-584
Gaskiers	Avalon Peninsula, Newfoundland	DB	580.0-581.9
Drook	Avalon Peninsula, Newfoundland	DB	570.6-580.0
Briscal	Avalon Peninsula, Newfoundland	DB	566.8-570.6
Mistaken Point	Avalon Peninsula, Newfoundland	DB	565.0-566.8
Trepassey	Avalon Peninsula, Newfoundland	DB	563.6-565.0
Fermeuse	Avalon Peninsula, Newfoundland	DB	556.0-563.6
Upper Staraya	Siberia	SS	565
Spiral Creek	East Greenland	SS	652-660

DB-Deep basin

OS-Outer shelf and shallow basin, all below mean storm wave base

SS-Shallow shelf, above mean storm wave base

Table 4. Calculated parameters from carbon isotope curves.

Time Period ^j (Ma)	^a $\delta^{13}\text{C}_{\text{IC}}$ ‰	^b $\delta^{13}\text{C}_{\text{cc}}$ ‰	^c $\delta^{13}\text{C}_{\text{IC-calc}}$ ‰	^d $\delta^{13}\text{C}_{\text{OC}}$ ‰	^e IC wt%	^f OC wt%	^g f_{cc}	^h f_{org}	ⁱ $f_{\text{org-cc}}$
Tonian (725-835)	3.97	3.81	3.88	-30.04	1.64	1.20	0.37	0.264	0.262
Cryogenian (652-660)	4.17	0.94	2.72	-29.14	2.02	0.56	0.45	0.275	0.242
Ediacaran (541-635)	1.12	-2.73	0.67	-29.80	0.52	0.24	0.112	0.198	0.186
Ediacaran 1 (541-560)	2.91	-7.97	2.64	-30.34	0.12	0.44	0.026	0.238	0.231
Ediacaran 2 (560-570)	-6.55	-1.81	-5.82	-27.02	0.69	0.10	0.15	-0.076	-0.039
Ediacaran 3 (570-635)	1.32	-3.81	0.84	-30.09	0.42	0.30	0.093	0.201	0.189
Neoproterozoic (541-840)	2.82	0.93	2.34	-30.16	1.13	0.80	0.250	0.237	0.226

^aaverage $\delta^{13}\text{C}$ (‰) for the standard isotope record (Figure 1)

^baverage $\delta^{13}\text{C}$ (‰) for the clastic rock-hosted (Figure 2)

^caverage $\delta^{13}\text{C}$ (‰) calculated for the given $f_{\text{org-cc}}$ (last column) but assuming no clastic rock carbonate formation. The difference between $\delta^{13}\text{C}_{\text{IC}}$ and $\delta^{13}\text{C}_{\text{IC-calc}}$ indicates the influence of clastic rock hosted carbonate on the $\delta^{13}\text{C}_{\text{IC}}$ of seawater

^daverage $\delta^{13}\text{C}$ (‰) for the clastic rock-hosted organic carbon (Figure 2)

^eaverage clastic rock hosted wt% IC (Figure 2)

^faverage clastic rock hosted wt% OC (Figure 2)

^gfraction of total IC buried as clastic rock-associated IC

^hfraction of total carbon buried as organic carbon without considering clastic rock hosted IC (equation 2).

ⁱfraction of total carbon buried as organic carbon considering clastic rock hosted IC (equation 4).

^jincluding time interval considered in our analysis

Figure Captions

Figure 1. Standard inorganic carbon isotope curve for the time interval 540 to 890 Ma. Also given are averages (red circles) binned in mostly 10 million-year intervals. For the Tonian Period, data is from (MacLennan and others, 2018) and (Swanson-Hysell and others, 2015) with the age model given in (MacLennan and others, 2018). Data from the Cryogenian Period is from (Cox and others, 2016), with the ages modified to reflect a 15 million year ice-free period extending from 645 to 660 Ma (Hoffman and others, 2017). For the post-Shuram Ediacaran Period, the data includes results from S. China (McFadden and others, 2008) with the chronology presented in (Macdonald and others, 2013) and until the unconformity at 551 Ma. The data also comes from Oman (Fike and others, 2006), with an age model such that the Shuram-Wonoka anomaly ends at 562 Ma as proposed here. Late Ediacaran data is from Morocco with the data and age model from (Macdonald and others, 2013). Data for the Shuram-Wonoka isotope excursion come from both Oman (Fike and others, 2006) and S. China (McFadden and others, 2008) assuming the excursion lasted from 562 to 568 Ma as proposed here. Pre-Shuram data is from Oman (Fike and others, 2006), with age model of (Cox and others, 2016), adjusted for the Shuram-Wonoka anomaly to begin at 569 Ma, and from S. China (McFadden and others, 2008) and Namibia (Halverson and others, 2005) following the age model of (Macdonald and others, 2013). Additional pre-Shuram data from Cox and others (2016).

Figure 2. A) isotope record of clastic rock-hosted inorganic carbon and organic carbon. B) concentrations of inorganic carbon from the analyzed sedimentary rocks. C) concentrations of organic carbon from the analyzed sedimentary rocks. Except for the isotopic composition of organic carbon, the data has been separated into different rock types.

Figure 3. A) The isotopic composition of clastic rock-inorganic carbon versus the concentration of organic carbon (TOC). The isotopic composition of clastic rock-inorganic carbon versus FeHR/FeT.

The iron speciation data is found in Table A1 and references (Canfield and others, 2008, Canfield, Poulton, and Narbonne, 2007).

Figure 4. A) The isotopic composition of clastic rock-carbonate from the Kaza-Isaac Formations from the Windermere Supergroup. Different methods (elemental analyzer and gas bench) were used to collect the isotope data as indicated. Also included in a dashed line are a generalization of the data trends present in Cochrane, Navarro, and Arnott (2019). All of these data are compared to the Shuram-Wonoka isotope anomaly as found in Oman. B) wt% clastic-rock associated inorganic carbon from two different methods as indicated. C) FeHR/FeT for clastic sedimentary rocks from the Isaac and Kaza formations. See text for details. The general stratigraphy of the sampled intervals is also indicated as well as the stratigraphic interval of the First Isaac Carbonate (FIC).

Figure 5. Isotopic composition of clastic rock IC for sedimentary rock of the Avalon Peninsula, Newfoundland. The formation boundaries are indicated, as well as dated intervals. Also indicated are suggestions for correlations to the Shuram-Wonoka anomaly and the EN2 anomaly. New date for the Trepassey Formation given in red. See text for details.

Figure 1

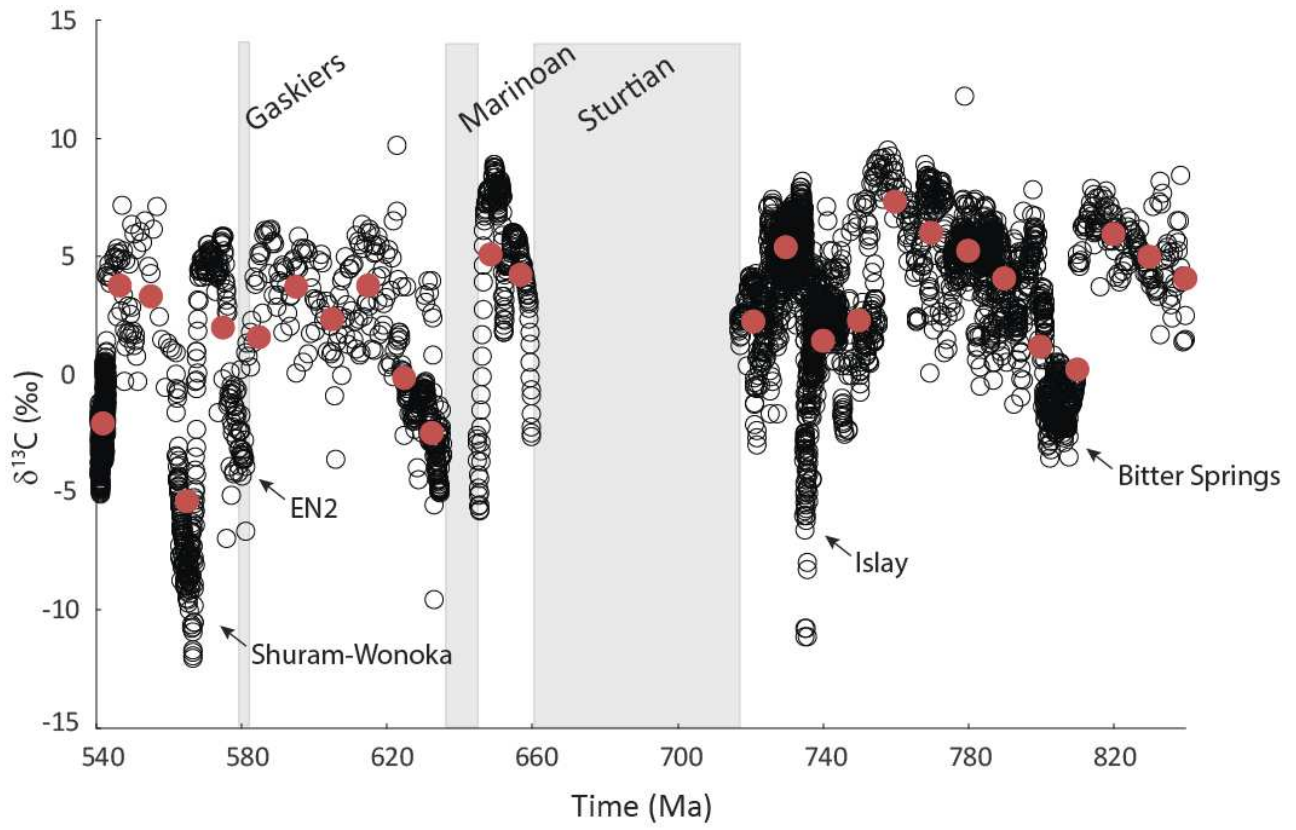


Figure 2

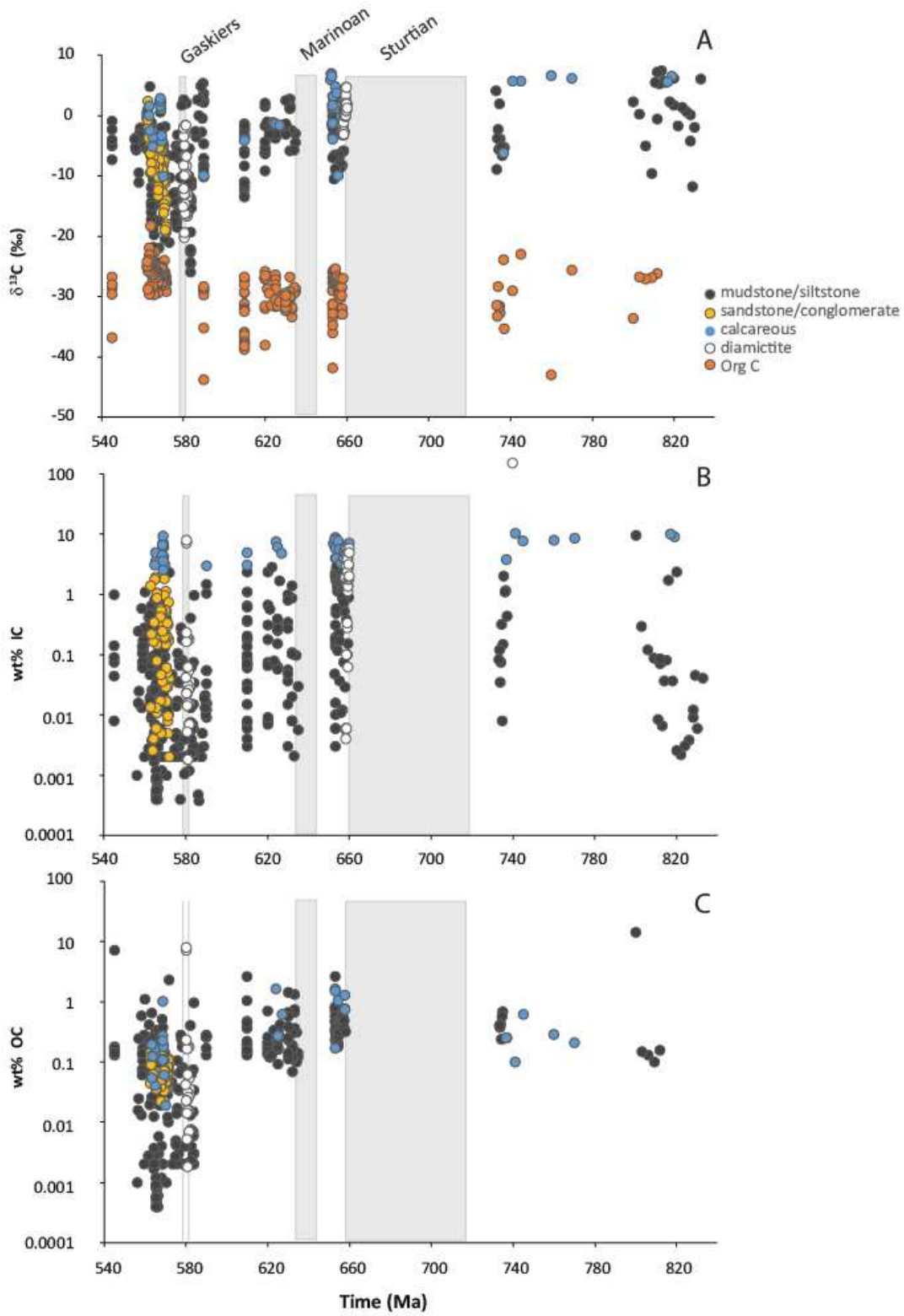


Figure 3

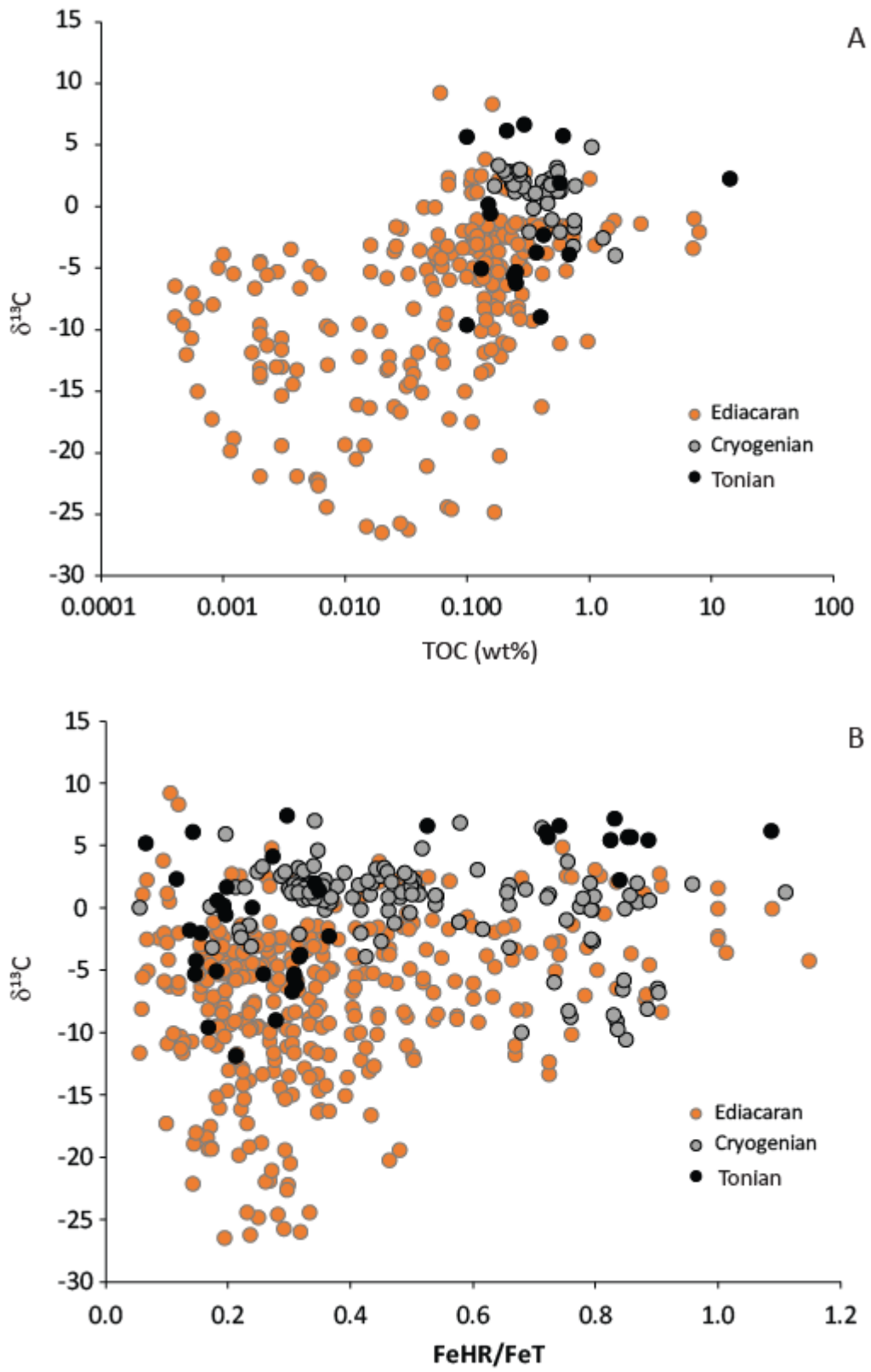


Figure 4.

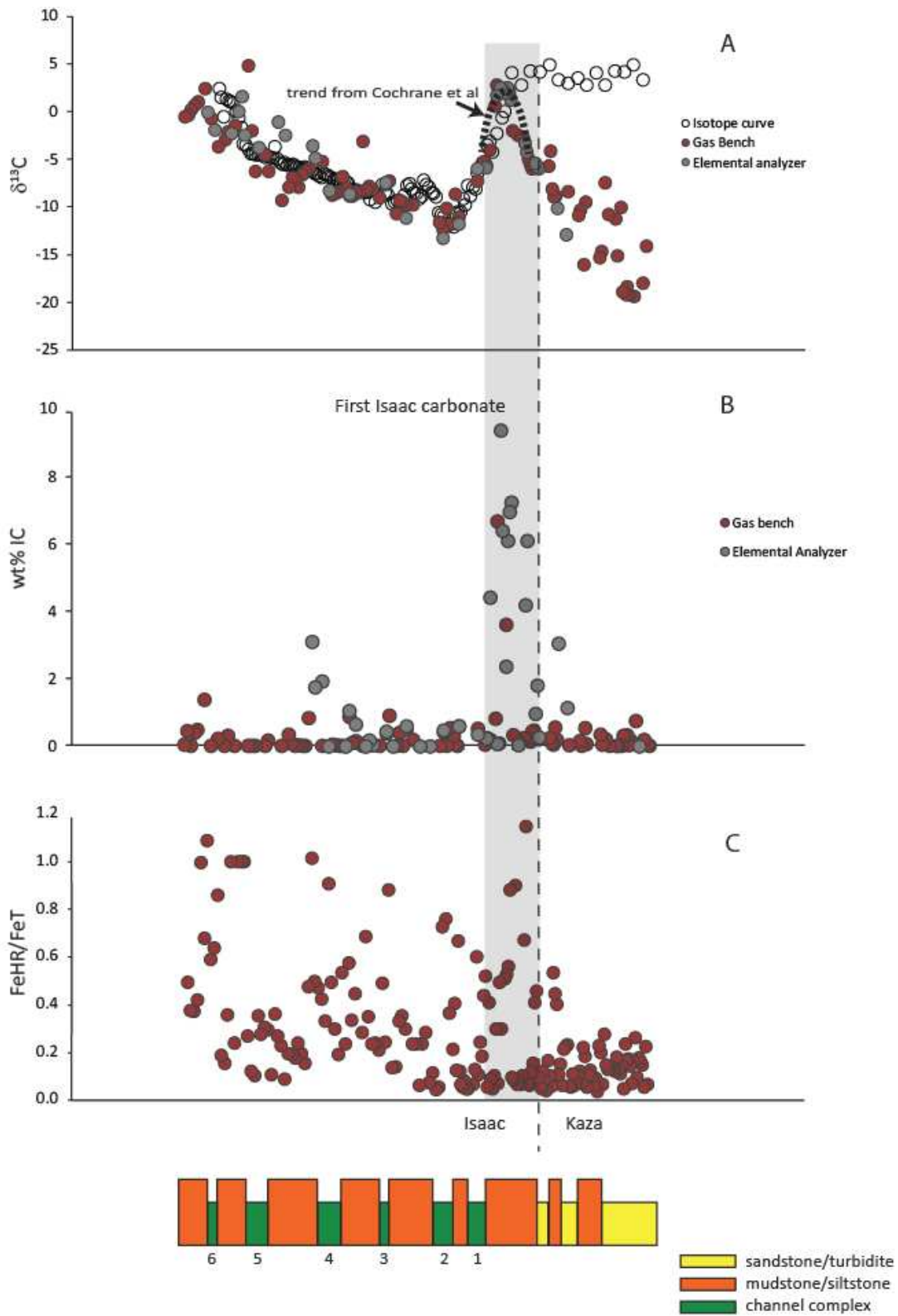
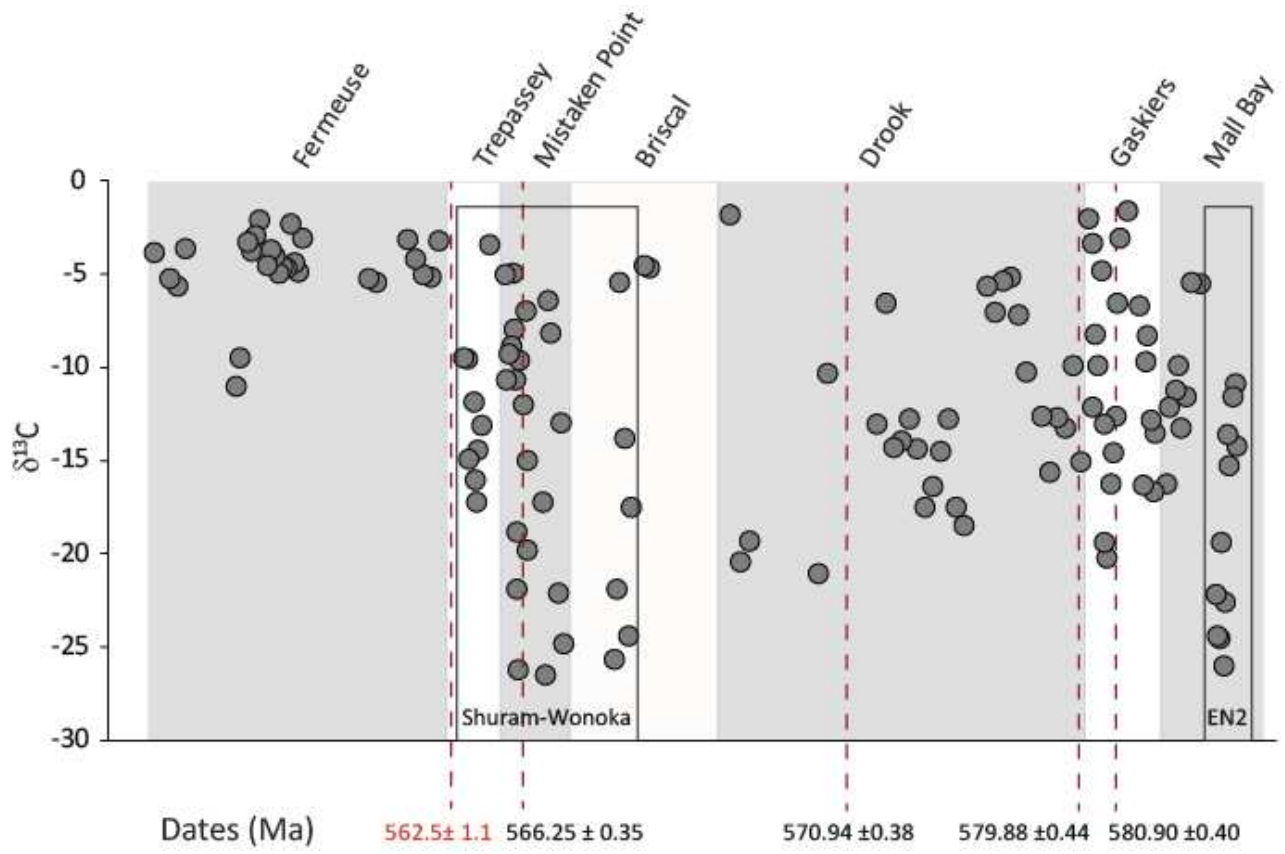


Figure 5



References

- Arnott, R., and Ross, G., 2007, Overview: Outcrop analysis of an ancient, passive margin, turbidite system: Windermere Supergroup, British Columbia, Canada: *Am Assoc Pet Geol Stud Geol*, v. 56, p. 81-84.
- Berner, R. A., 2004, *The Phanerozoic Carbon Cycle: CO₂ and O₂*: Oxford, Oxford University Press, 150 p.
- Berner, R. A., 2006, GEOCARBSULF: A combined model for Phanerozoic atmospheric O₂ and CO₂: *Geochimica et Cosmochimica Acta*, v. 70, p. 5653-5664.
- Berner, R. A., and Canfield, D. E., 1989, A new model for atmospheric oxygen over Phanerozoic time: *American Journal of Science*, v. 289, p. 333-361.
- Berner, R. A., and Raiswell, R., 1983, Burial of organic carbon and pyrite sulfur in sediment over Phanerozoic time: a new theory: *Geochimica et Cosmochimica Acta*, v. 47, p. 855-862.
- Bjerrum, C. J., and Canfield, D. E., 2004a, New insights into the burial history of organic carbon on the early Earth: *Geochemistry Geophysics Geosystems*, v. 5, p. Q08001, doi:10.1029/2004GC000713.
- Bjerrum, C. J., and Canfield, D. E., 2004b, New insights into the burial history of organic carbon on the early Earth: *Geochemistry Geophysics Geosystems*, v. 5, p. 9.
- , 2011, Towards a quantitative understanding of the late Neoproterozoic carbon cycle: *Proceedings of the National Academy of Sciences of the United States of America*, v. 108, p. 5542-5547.
- Bobrovskiy, I., Hope, J. M., Ivantsov, A., Nettersheim, B. J., Hallmann, C., and Brocks, J. J., 2018, Ancient steroids establish the Ediacaran fossil Dickinsonia as one of the earliest animals: *Science*, v. 361, p. 1246-1249.
- Buick, R., Des Maris, D. J., and Knoll, A. H., 1995, Stable isotopic composition of carbonates from the Mesoproterozoic Bangemall Group, northwestern Australia: *Chemical Geology*, v. 123, p. 153-171.
- Canfield, D. E., 2005, The early history of atmospheric oxygen: Homage to Robert M. Garrels: *Annual Review of Earth and Planetary Science*, v. 33, p. 1-36.
- Canfield, D. E., 2014, Proterozoic atmospheric oxygen, *in* Farquhar, J., editor, *Treatise on Geochemistry, Atmosphere-History*: Amsterdam, Elsevier.

- Canfield, D. E., Poulton, S. W., Knoll, A. H., Narbonne, G. M., Ross, G., Goldberg, T., and Strauss, H., 2008, Ferruginous conditions dominated later Neoproterozoic deep water chemistry: *Science*, v. 321, p. 949-952.
- Canfield, D. E., Poulton, S. W., and Narbonne, G. M., 2007, Late-Neoproterozoic deep-ocean oxygenation and the rise of animal life: *Science*, v. 315, p. 92-95.
- Canfield, D. E., and Raiswell, R., 1991, Carbonate precipitation and dissolution: Its relevance to fossil preservation, *in* Allison, P. A., and Briggs, D. E. G., editors, *Topics in Geobiology*: New York, Plenum Press, p. 411-453.
- Cochrane, D. J., Navarro, L., and Arnott, R. W. C., 2019, Sedimentological and geochemical evolution of an Ediacaran mixed carbonate-siliciclastic continental slope system, Windermere Supergroup, southern Canadian Cordillera, British Columbia, Canada: *Precambrian Research*, v. 327, p. 47-67.
- Condon, D., Zhu, M., Bowring, S., Wang, W., and Yang, J., 2005, U-Pb ages from the Neoproterozoic Doushantuo Formation, China: *Science*, v. 308, p. 95-98.
- Cox, G. M., Halverson, G. P., Stevenson, R. K., Vokaty, M., Poirier, A., Kunzmann, M., Li, Z.-X., Denyszyn, S. W., Strauss, J. V., and Macdonald, F. A., 2016, Continental flood basalt weathering as a trigger for Neoproterozoic Snowball Earth: *Earth and Planetary Science Letters*, v. 446, p. 89-99.
- Deines, P., 1980, The carbon isotopic composition of diamonds: relationship to diamond shape, color, occurrence and vapor composition: *Geochimica et Cosmochimica Acta*, v. 44, p. 943-961.
- Derry, L. A., 2010, A burial diagenesis origin for the Ediacaran Shuram-Wonoka carbon isotope anomaly: *Earth and Planetary Science Letters*, v. 294, p. 152-162.
- Des Marais, D. J., Strauss, H., Summons, R. E., and Hayes, J. M., 1992, Carbon isotope evidence for the stepwise oxidation of the Proterozoic environment: *Nature*, v. 359, p. 605-609.
- Eyles, N., and Eyles, C. H., 1989, Glacially - influenced deep - marine sedimentation of the Late Precambrian Gaskiers Formation, Newfoundland, Canada: *Sedimentology*, v. 36, p. 601-620.

- Fike, D. A., Grotzinger, J. P., Pratt, L. M., and Summons, R. E., 2006, Oxidation of the Ediacaran Ocean: *Nature*, v. 444, p. 744-747.
- Gardiner, S., and Hiscott, R. N., 2003, Deep-water facies and depositional setting of the lower conception group (Hadrynian), southern Avalon Peninsula, Newfoundland: *Canadian Journal of Earth Sciences*, v. 25, p. 1579-1594.
- Garrels, R. M., and Lerman, A., 1981, Phanerozoic cycles of sedimentary carbon and sulfur: *Proceedings of the National Academy of Sciences of the United States of America*, v. 78, p. 4652-4656.
- Garrels, R. M., and Perry, E. A., 1974, Cycling of carbon, sulfur, and oxygen through geologic time, *in* Goldberg, E. D., editor, *The Sea*: New York, John Wiley and Sons, p. 303-336.
- Gehling, J. G., Narbonne, G. M., and Anderson, M. M., 2000, The first named Ediacaran body fossil, *Aspidella terranovica*: *Palaeontology*, v. 43, p. 427-456.
- Geyman, E. C., and Maloof, A. C., 2019, A diurnal carbon engine explains ^{13}C -enriched carbonates without increasing the global production of oxygen: *Proceedings of the National Academy of Sciences*.
- Grotzinger, J. P., Fike, D. A., and Fischer, W. W., 2011, Enigmatic origin of the largest-known carbon isotope excursion in Earth's history: *Nature Geoscience*, v. 4, p. 285-292.
- Halverson, G. P., Hoffmann, P. F., Schrag, D. P., Maloof, A. C., and Rice, A. H., 2005, Towards a Neoproterozoic composite carbon isotope record: *Geological Society of America Bulletin*, v. 117, p. 1181-1207.
- Hayes, J. M., Strauss, H., and Kaufman, A. J., 1999, The abundance of ^{13}C in marine organic matter and isotopic fractionation in the global biogeochemical cycle of carbon during the past 800 Ma: *Chemical Geology*, v. 161, p. 103-125.
- Hoffman, P. F., Abbot, D. S., Ashkenazy, Y., Benn, D. I., Brocks, J. J., Cohen, P. A., Cox, G. M., Creveling, J. R., Donnadieu, Y., and Erwin, D. H., 2017, Snowball Earth climate dynamics and Cryogenian geology-geobiology: *Science Advances*, v. 3, p. e1600983.

- Hoffman, P. F., and Lamothe, K. G., 2019, Seawater-buffered diagenesis, destruction of carbon isotope excursions, and the composition of DIC in Neoproterozoic oceans: *Proceedings of the National Academy of Sciences*, v. 116, p. 18874-18879.
- Husson, J. M., Maloof, A. C., and Schoene, B., 2012, A syn - depositional age for Earth's deepest $\delta^{13}\text{C}$ excursion required by isotope conglomerate tests: *Terra Nova*, v. 24, p. 318-325.
- Husson, J. M., Maloof, A. C., Schoene, B., Chen, C. Y., and Higgins, J. A., 2015, Stratigraphic expression of Earth's deepest $\delta^{13}\text{C}$ excursion in the Wonoka Formation of South Australia: *American Journal of Science*, v. 315, p. 1-45.
- Jaffey, A., Flynn, K., Glendenin, L., Bentley, W. t., and Essling, A., 1971, Precision measurement of half-lives and specific activities of U 235 and U 238: *Physical review C*, v. 4, p. 1889.
- Kaufman, A. J., Knoll, A. H., and Narbonne, G. M., 1997, Isotopes, ice ages and terminal proterozoic earth history: *Proceedings of National Academy of Sciences USA*, v. 94, p. 6600-6605.
- Kendall, B. S., Creaser, R. A., Ross, G. M., and Selby, D., 2004, Constraints on the timing of Marinoan "Snowball Earth" glaciation by ^{187}Re - ^{187}Os dating of a Neoproterozoic, post-glacial black shale in Western Canada: *Earth and Planetary Science Letters*, v. 222, p. 729-740.
- Knauth, L. P., and Kennedy, M. J., 2009, The late Precambrian greening of the Earth: *Nature*, v. 460, p. 728-732.
- Knoll, A., Kaufman, A., and Semikhatov, M., 1995, The Proterozoic carbon isotopic record: Mesoproterozoic carbonates from Siberia: *American Journal of Science*, v. 295, p. 823-850.
- Knoll, A. H., 2014, Paleobiological perspectives on early eukaryotic evolution: *Cold Spring Harbor Perspectives in Biology*, p. 1-14.
- Knoll, A. H., Hayes, J. M., Kaufman, A. J., Swett, K., and Lambert, I. B., 1986, Secular variation in carbon isotope ratios from Upper Proterozoic successions of Svalbard and East Greenland: *Nature*, v. 321, p. 832-838.

- Krogh, T., 1973, A low-contamination method for hydrothermal decomposition of zircon and extraction of U and Pb for isotopic age determinations: *Geochimica et Cosmochimica Acta*, v. 37, p. 485-494.
- Liu, A. G., Kenchington, C. G., and Mitchell, E. G., 2015, Remarkable insights into the paleoecology of the Avalonian Ediacaran macrobiota: *Gondwana Research*, v. 27, p. 1355-1380.
- Macdonald, F. A., Strauss, J. V., Sperling, E. A., Halverson, G. P., Narbonne, G. M., Johnston, D. T., Kunzmann, M., Schrag, D. P., and Higgins, J. A., 2013, The stratigraphic relationship between the Shuram carbon isotope excursion, the oxygenation of Neoproterozoic oceans, and the first appearance of the Ediacara biota and bilaterian trace fossils in northwestern Canada: *Chemical Geology*, v. 362, p. 250-272.
- MacLennan, S., Park, Y., Swanson-Hysell, N., Maloof, A., Schoene, B., Gebreslassie, M., Antilla, E., Tesema, T., Alene, M., and Haileab, B., 2018, The arc of the Snowball: U-Pb dates constrain the Islay anomaly and the initiation of the Sturtian glaciation: *Geology*, v. 46, p. 539-542.
- Mattinson, J. M., 2005, Zircon U–Pb chemical abrasion (“CA-TIMS”) method: combined annealing and multi-step partial dissolution analysis for improved precision and accuracy of zircon ages: *Chemical Geology*, v. 220, p. 47-66.
- McFadden, K. A., Huang, J., Chu, X. L., Jiang, G. Q., Kaufman, A. J., Zhou, C. M., Yuan, X. L., and Xiao, S. H., 2008, Pulsed oxidation and biological evolution in the Ediacaran Doushantuo Formation: *Proceedings of the National Academy of Sciences of the United States of America*, v. 105, p. 3197-3202.
- Mills, D. B., Francis, W. R., and Canfield, D. E., 2018, Animal origins and the Tonian Earth system: *Emerging Topics in Life Sciences*, v. 2, p. 289-298.
- Minguez, D., Kodama, K., and Hillhouse, J., 2015, Paleomagnetic and cyclostratigraphic constraints on the synchronicity and duration of the Shuram carbon isotope excursion, Johnnie Formation, Death Valley Region, CA: *Precambrian Research*, v. 266, p. 395-408.

- Narbonne, G. M., 2005, The ediacara biota: Neoproterozoic origin of animals and their ecosystems: Annual Review of Earth and Planetary Science, v. 33, p. 421-442.
- Narbonne, G. M., Laflamme, M., Trusler, P. W., Dalrymple, R. W., and Greentree, C., 2014, Deep-water Ediacaran fossils from northwestern Canada: taphonomy, ecology, and evolution: Journal of Paleontology, v. 88, p. 207-223.
- Narbonne, G. M., Xiao, S., and Shields, G. A., 2012, The Ediacaran Period, in Gradstein, F. M., Ogg, J. G., Schmitz, M. D., and Ogg, G. M., editors, Geologic Timescale 2012: Amsterdam, Elsevier, p. 413–435.
- Navarro, L., Khan, Z., and Arnott, R. W. C., 2007, Depositional architecture and evolution of a deep-marine channel-levee complex: Isaac Formation (Windermere Supergroup), southern Canadian Cordillera: Atlas of deep-water outcrops: AAPG Studies in Geology, v. 56, p. 79-108.
- O'Brien, S., and King, A., 2005, Late Neoproterozoic (Ediacaran) stratigraphy of Avalon Zone sedimentary rocks, Bonavista Peninsula, Newfoundland: Current Research, Newfoundland and Labrador Department of Natural Resources Geological Survey, v. 5, p. 101-113.
- Planavsky, N. J., McGoldrick, P., Scott, C. T., Li, C., Reinhard, C. T., Kelly, A. E., Chu, X., Bekker, A., Love, G. D., and Lyons, T. W., 2011, Widespread iron-rich conditions in the mid-Proterozoic ocean: Nature, v. 477, p. 448-451.
- Planavsky, N. J., Reinhard, C. T., Wang, X., Thomson, D., McGoldrick, P., Rainbird, R. H., Johnson, T., Fischer, W. W., and Lyons, T. W., 2014, Low Mid-Proterozoic atmospheric oxygen levels and the delayed rise of animals: Science, v. 346, p. 635-638.
- Poulton, S. W., and Canfield, D. E., 2011, Ferruginous Conditions: A Dominant Feature of the Ocean through Earth's History: Elements, v. 7, p. 107-112.
- Pu, J. P., Bowring, S. A., Ramezani, J., Myrow, P., Raub, T. D., Landing, E., Mills, A., Hodgkin, E., and Macdonald, F. A., 2016, Dodging snowballs: Geochronology of the Gaskiers glaciation and the first appearance of the Ediacaran biota: Geology, v. 44, p. 955-958.

- Raiswell, R., and Canfield, D. E., 1998, Sources of iron for pyrite formation in marine sediments: *American Journal of Science*, v. 298, p. 219-245.
- , 2012, *The Iron Biogeochemical Cycle Past and Present Geochemical Perspectives*, v. 1, p. 1-220.
- Ross, G. M., Bloch, J. D., and Krouse, H. R., 1995, Neoproterozoic strata of the southern Canadian Corallera and the isotopic evolution of seawater sulfate: *Precambrian Research*, v. 73, p. 71-99.
- Rothman, D. H., Hayes, J. M., and Summons, R. E., 2003, Dynamics of the Neoproterozoic carbon cycle: *PNAS*, v. 100, p. 8124-8129.
- Schrag, D. P., Higgins, J. A., Macdonald, F. A., and Johnston, D. T., 2013, Authigenic carbonate and the history of the global carbon cycle: *Science*, v. 339, p. 540-543.
- Scott, C., Lyons, T. W., Bekker, A., Shen, Y., Poulton, S. W., Chu, X., and Anbar, A. D., 2008, Tracing the stepwise oxygenation of the Proterozoic ocean: *Nature*, v. 452, p. 456-459.
- Sperling, E. A., Knoll, A. H., and Girguis, P. R., 2015, The ecological physiology of earth's second oxygen revolution *Reviews in Advance*, p. 215-235.
- Sperling, E. A., and Stockey, R. G., 2018, The temporal and environmental context of early animal evolution: considering all the ingredients of an "Explosion": *Integrative and comparative biology*, v. 58, p. 605-622.
- Stacey, J. t., and Kramers, J., 1975, Approximation of terrestrial lead isotope evolution by a two-stage model: *Earth and planetary science letters*, v. 26, p. 207-221.
- Swanson-Hysell, N. L., Maloof, A. C., Condon, D. J., Jenkin, G. R., Alene, M., Tremblay, M. M., Tesema, T., Rooney, A. D., and Haileab, B., 2015, Stratigraphy and geochronology of the Tambien Group, Ethiopia: evidence for globally synchronous carbon isotope change in the Neoproterozoic: *Geology*, v. 43, p. 323-326.
- Swart, P. K., and Kennedy, M., 2012, Does the global stratigraphic reproducibility of $\delta^{13}\text{C}$ in Neoproterozoic carbonates require a marine origin? A Pliocene–Pleistocene comparison: *Geology*, v. 40, p. 87-90.

- Torres, M. E., Mix, A. C., and Rugh, W. D., 2005, Precise $\delta^{13}\text{C}$ analysis of dissolved inorganic carbon in natural waters using automated headspace sampling and continuous - flow mass spectrometry: *Limnology and Oceanography: Methods*, v. 3, p. 349-360.
- Von Strandmann, P. A. P., Stüeken, E. E., Elliott, T., Poulton, S. W., Dehler, C. M., Canfield, D. E., and Catling, D. C., 2015, Selenium isotope evidence for progressive oxidation of the Neoproterozoic biosphere: *Nature communications*, v. 6, p. 10157.
- Wang, X., Zhang, S., Wang, H., Bjerrum, C. J., Hammarlund, E. U., Haxen, E. R., Su, J., Wang, Y., and Canfield, D. E., 2017, Oxygen, climate and the chemical evolution of a 1400 million year old tropical marine setting: *American Journal of Science*, v. 317, p. 861-900.
- Wilson, A. M., 2005, Fresh and saline groundwater discharge to the ocean: A regional perspective: *Water Resources Research*, v. 41.
- Wood, D. A., 2003, Facies and paleoenvironmental dynamics of the terminal Neoproterozoic Mistaken Point and Trepassey formations, southeastern Newfoundland: M.Sc., Queen's University, Kingston, Ontario, p.
- Wood, D. A., Dalrymple, R. W., Narbonne, G. M., Gehling, J. G., and Clapham, M. E., 2003, Paleoenvironmental analysis of the late Neoproterozoic Mistaken Point and Trepassey formations, southeastern Newfoundland: *Canadian Journal of Earth Sciences*, v. 40, p. 1375-1391.
- Xiao, S., Narbonne, G. M., Zhou, C., Laflamme, M., Grazhdankin, D. V., Moczyłowska-Vidal, M., and Cui, H., 2016, Towards an Ediacaran time scale: problems, protocols, and prospects: *Episodes*, v. 39, p. 540-555.
- Zhou, M., Luo, T., Huff, W. D., Yang, Z., Zhou, G., Gan, T., Yang, H., and Zhang, D., 2018, Timing the termination of the Doushantuo negative carbon isotope excursion: evidence from U-Pb ages from the Dengying and Liuchapo formations, South China: *Science Bulletin*, v. 63, p. 1431-1438.

Appendix

Dating ash Layer in Trepassey Fm; Location, description, U/Pb Zircon CA-TIMS Analytical Procedure and Age

The ash is 8 cm thick and yellowish grey; it is graded with the dated sample obtained from the basal centimeter of the bed. The sample was collected at Shingle Head in the Mistaken Point Ecological Reserve from a location near the eastern end of section 4 (Wood and others, 2003); their Fig. 1). The Trepassey Formation at Shingle Head accumulated on a deep-water slope and consists of thin-bedded distal turbidites, synsedimentary slides and slumps composed of these distal turbidites, and sporadic beds of volcanic ash (Wood and others, 2003). The dated ash occurs 27 m below the top of the Trepassey Formation, 16.7 m below the Shingle Head fossil surface located at the 179 m mark (Wood and others, 2003); their Fig. 4A), in a slide mass of distal turbidites. The ash is stratigraphically bracketed by carbon-isotope values of approximately -9.5‰ (samples 43 and 45 in Table A1) in turbidites below and above the slide mass

This sample yielded small prismatic zircon that appear to represent a single- age igneous population displaying fine scale growth zoning in some crystals, and low luminescence in most (Figure 1). This is confirmed by the overlapping concordant analyses on Figure 2.

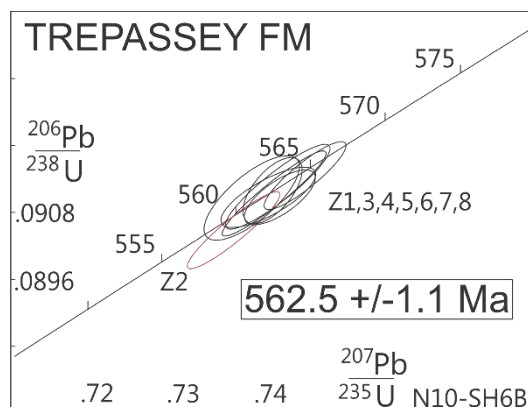
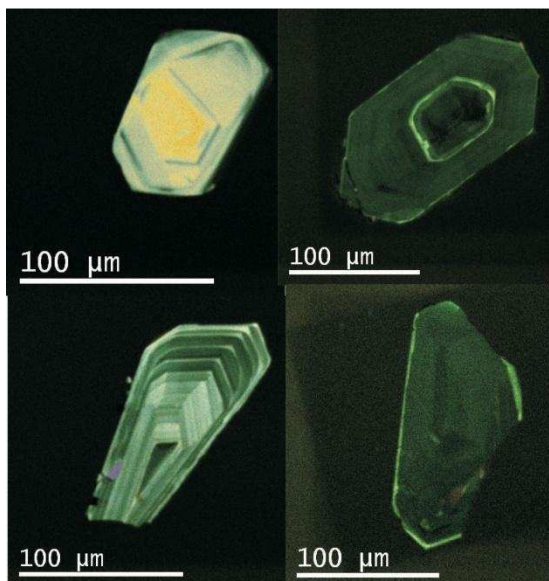


Fig. 1 Cathode- luminescence images of typical zircon

Fig.2 Concordia Diagram with data for Trepassey Ash

The zircon grains analysed were selected from mineral concentrates using tweezers under the microscope according to criteria of clarity, euhedral crystal form and lack of inclusions. All grains were chemically abraded using the (Mattinson, 2005) chemical abrasion thermal ionization mass spectrometry (CA-TIMS) technique. The selected crystals of zircon were annealed at 1000° C for 36 hours prior to etching in concentrated HF acid in a pressure bomb at 200° C for a few hours. This procedure is designed to remove any altered domains throughout the crystal that may have undergone lead loss.

A small number of zircon grains were grouped into fractions to allow precise measurement of all Pb masses on the mass spectrometer. These etched zircon fractions were washed in distilled HNO₃, then doubly distilled H₂O, prior to loading in Krogh- type TEFLON dissolution bombs. A mixed ²⁰⁵Pb/²³⁵U tracer was added in proportion to the sample weight, along with ca. 15 drops of distilled HF, then the bomb was sealed and placed in an oven at 210°C for 5 days. Ion exchange chemistry was carried out according to the procedure of (Krogh, 1973), with modified columns and reagent volumes scaled down to one tenth of those reported in 1973. The purified Pb and U were collected in a clean beaker in a single drop of ultrapure H₃PO₄.

Lead and uranium are loaded together on outgassed single Re filaments with silica gel and dilute H₃PO₄. Mass spectrometry is carried out using a multi-collector MAT 262. The faraday cups are calibrated with NBS 981 lead standard and the ion-counting secondary electron multiplier (SEM) detector is calibrated against the faraday cups by measurement of known lead isotopic ratios. The small amounts of Pb were measured by peak jumping on the SEM, with measurement times weighted according to the amounts of each mass present. U was measured by peak jumping on the SEM. A series of sets of data were measured in the temperature range 1400 to 1550°C for Pb and 1550 to 1640°C for U, and the best sets combined to produce a mean value for each ratio. The measured ratios are corrected for Pb and U fractionation of 0.1% /amu and 0.03%/amu respectively as determined from repeat measurements of NBS standards. The ratios are also corrected for laboratory procedure blanks (1-2 picograms - Pb, 0.3 picogram - U) and for common lead above the laboratory blank with lead of the composition predicted by the two- stage model of (Stacey and Kramers, 1975) for the age of the sample. Ages are calculated using the decay constants recommended by (Jaffey and others, 1971). The uncertainties on the isotopic ratios and ages are calculated using an unpublished program and are reported as two sigma in Table A1.

The final age of 562.5 +/-1.1 Ma is the weighted average of the ²⁰⁶Pb/²³⁸U ages for analyses Z1, and Z3 – Z8, and is reported at the 95% confidence interval (ISOPLOT, MSWD = 0.34). Z2 was excluded as it appears to exhibit a small degree (0.5%) of lead- loss.

See supplement Tables for data from this study and for “standard” carbon isotope compilation.

TABLE A3. U-Pb Zircon Data for Sample N10-SH6B

Fraction	Weight [mg]	Concentration		Measured		Corrected Atomic Ratios*						Age [Ma]			
		U [ppm]	Pb rad	total common Pb [pg]	206Pb ----- 204Pb	208Pb ----- 206Pb	206Pb ----- 238U	207Pb ----- 235U	207Pb ----- 206Pb	206Pb ----- 238U	207Pb ----- 235U	207Pb ----- 206Pb	+/-	+/-	+/-
Z1 5 clr euh prm	0.007	1656	153.7	13	5350	0.1245	0.09117	62	0.7408	48	0.05893	14	562.4	563	565
Z2 4 clr euh prm	0.006	850	78.5	3.2	9078	0.1274	0.09051	56	0.7361	44	0.05899	14	559	560	567
Z3 3 clr euh prm	0.004	958	89.3	4.0	6170	0.1248	0.09149	50	0.7443	38	0.05900	14	564.4	565	567
Z4 2 clr euh prm	0.003	580	53.8	2.5	4004	0.1251	0.09110	40	0.7414	34	0.05903	20	562.1	563	568
Z5 4 clr euh prm	0.006	634	58.7	3.1	7074	0.1193	0.09129	62	0.7412	50	0.05889	18	563.0	563	563
Z6 3 stubby euh prm	0.004	520	48.0	4.9	2747	0.1201	0.09109	44	0.7401	44	0.05893	24	561.8	562	564
Z7 2 stubby euh prm	0.003	801	74.7	4.4	3146	0.1318	0.09109	62	0.7382	44	0.05878	28	561.8	561	559
Z8 4 clr euh prm	0.006	668	62.0	2.9	7814	0.1235	0.09122	48	0.7406	28	0.05888	24	562.6	563	563

Notes: Z=zircon, 2,4,5 =number of grains, clr=clear, prm =prism, euh=euhedral

All zircon was chemically abraded (Mattinson, 2005). Weights were estimated so U and Pb concentrations are approximate.

* Atomic ratios corrected for fractionation, spike, laboratory blank of 1-2 picograms of common lead, and initial common lead at the age of the sample calculated from the model of Stacey and Kramers (1975), and 0.3 picogram U blank. Two sigma uncertainties are reported after the ratios and refer to the final digits. Ages used in the age calculation are reported to the first decimal place.

